



# 1 On the sources and sinks of atmospheric VOCs: An integrated 2 analysis of recent aircraft campaigns over North America

3 Xin Chen<sup>1</sup>, Dylan B. Millet<sup>1</sup>, Hanwant B. Singh<sup>2</sup>, Armin Wisthaler<sup>3,4</sup>, Eric C. Apel<sup>5</sup>, Elliot L.  
4 Atlas<sup>6</sup>, Donald R. Blake<sup>7</sup>, Steven S. Brown<sup>8</sup>, John D. Crouse<sup>9</sup>, Joost A. de Gouw<sup>8,10</sup>, Frank  
5 Flocke<sup>5</sup>, Alan Fried<sup>11</sup>, Brian G. Heikes<sup>12</sup>, Rebecca S. Hornbrook<sup>5</sup>, Tomas Mikoviny<sup>4</sup>, Kyung-Eun  
6 Min<sup>13</sup>, Markus Müller<sup>3,\*</sup>, J. Andrew Neuman<sup>8,10</sup>, Daniel W. O'Sullivan<sup>14</sup>, Jeff Peischl<sup>8,10</sup>,  
7 Gabriele G. Pfister<sup>5</sup>, Dirk Richter<sup>12</sup>, James M. Roberts<sup>8</sup>, Thomas B. Ryerson<sup>8</sup>, Stephen Shertz<sup>15</sup>,  
8 Victoria Treadaway<sup>12</sup>, Patrick R. Veres<sup>8</sup>, James Walega<sup>11</sup>, Carsten Warneke<sup>8,10</sup>, Rebecca A.  
9 Washenfelder<sup>8</sup>, Petter Weibring<sup>11</sup>, Bin Yuan<sup>16</sup>

10 <sup>1</sup>Department of Soil, Water, and Climate, University of Minnesota, Minneapolis-Saint Paul, MN 55108, USA

11 <sup>2</sup>NASA Ames Research Center, Moffett Field, CA, USA

12 <sup>3</sup>Institute for Ion Physics and Applied Physics, University of Innsbruck, 6020 Innsbruck, Austria

13 <sup>4</sup>Department of Chemistry, University of Oslo, Norway

14 <sup>5</sup>Atmospheric Chemistry Observations & Modeling Laboratory, National Center for Atmospheric Research,

15 Boulder, CO, 80301, USA

16 <sup>6</sup>Department of Atmospheric Sciences, Rosenstiel School of Marine and Atmospheric Science, University of Miami,  
17 Miami, FL, USA

18 <sup>7</sup>Department of Chemistry, University of California, Irvine, Irvine, CA, USA

19 <sup>8</sup>Chemical Sciences Division, NOAA Earth System Research Laboratory, Boulder, CO 80305, USA

20 <sup>9</sup>Division of Geological and Planetary Sciences, California Institute of Technology, Pasadena, CA 91125, USA

21 <sup>10</sup>Cooperative Institute for Research in Environmental Sciences, University of Colorado, Boulder, CO 80309, USA

22 <sup>11</sup>Institute of Arctic & Alpine Research, University of Colorado, Boulder, CO

23 <sup>12</sup>Graduate School of Oceanography, University of Rhode Island, Narragansett, RI 02882, USA

24 <sup>13</sup>School of Earth Science and Environmental Engineering, Gwangju Institute of Science and Technology

25 <sup>14</sup>United States Naval Academy, Chemistry Department, Annapolis, MD, 21401, USA

26 <sup>15</sup>Atmospheric Chemistry Division, National Center for Atmospheric Research, Boulder, Colorado, USA

27 <sup>16</sup>Institute for Environmental and Climate Research, Jinan University, Guangzhou, China

28 \*now at: Ionicon Analytik GmbH, Innsbruck, Austria

29 *Correspondence to:* Dylan B. Millet ([dbm@umn.edu](mailto:dbm@umn.edu))

## 30 **Abstract**

31 We apply a high-resolution chemical transport model (GEOS-Chem CTM) with updated treatment of  
32 volatile organic compounds (VOCs) and a comprehensive suite of airborne datasets over North America  
33 to i) characterize the VOC budget, and ii) test the ability of current models to capture the distribution and  
34 reactivity of atmospheric VOCs, over this region. Biogenic emissions dominate the North American VOC  
35 budget in the model, accounting for 70% and 95% of annually emitted VOC-carbon and reactivity,  
36 respectively. Based on current inventories anthropogenic emissions have declined to the point where  
37 biogenic emissions are the dominant summertime source of VOC reactivity even in most major North  
38 American cities. Methane oxidation is a 2× larger source of non-methane VOCs (via production of  
39 formaldehyde and methyl hydroperoxide) over North America in the model than are anthropogenic  
40 emissions. However, anthropogenic VOCs account for over half the ambient VOC loading over the  
41 majority of the region owing to their longer aggregate lifetime. Fires can be a significant VOC source  
42 episodically but are small on average. In the planetary boundary layer (PBL), the model exhibits skill in  
43 capturing observed variability in total VOC-abundance ( $R^2 = 0.36$ ) and reactivity ( $R^2 = 0.54$ ). The same is



44 not true in the free troposphere (FT), where skill is low and there is a persistent low model bias (~60%),  
45 with most (27 of 34) model VOCs underestimated by more than a factor of 2. A comparison of PBL:FT  
46 concentration ratios over the southeastern US points to a misrepresentation of PBL ventilation as a  
47 contributor to these model FT biases. We also find that a relatively small number of VOCs (acetone,  
48 methanol, ethane, acetaldehyde, formaldehyde, isoprene + oxidation products, methyl hydroperoxide)  
49 drive a large fraction of total ambient VOC reactivity and associated model biases; research to improve  
50 understanding of their budgets is thus warranted. A source tracer analysis suggests a current overestimate  
51 of biogenic sources for hydroxyacetone, methyl ethyl ketone and glyoxal, an underestimate of biogenic  
52 formic acid sources, and an underestimate of peroxyacetic acid production across biogenic and  
53 anthropogenic precursors. Future work to improve model representations of vertical transport and to  
54 address the VOC biases discussed are needed to advance predictions of ozone and SOA formation.

55

## 56 1. Introduction

57 Volatile organic compounds (VOCs) play a central role in atmospheric chemistry. Through their influence  
58 on the hydroxyl radical (OH), VOCs alter the lifetime of long-lived greenhouse gases (Cubasch et al.,  
59 2013), while their oxidation products such as ozone (O<sub>3</sub>) and secondary organic aerosols (SOA) degrade  
60 human and ecosystem health (EPA, 2018) and alter Earth's radiative balance (Myhre et al., 2013). There  
61 are large uncertainties associated with the emissions (Karl et al., 2018; Hatch et al., 2017; Guenther et al.,  
62 2012), chemical processing (Caravan et al., 2018; Shaw et al., 2018; Müller et al., 2016a), and sinks of  
63 atmospheric VOCs (Iavorivska et al., 2017; Nguyen et al., 2015; Wolfe et al., 2015; Karl et al., 2010). An  
64 ensemble of recent airborne campaigns over North America together afford the most expansive picture  
65 yet of the atmospheric VOC distribution over this region. Here we apply a high-resolution chemical  
66 transport model (nested GEOS-Chem CTM) with a new and highly comprehensive VOC treatment to 1)  
67 interpret that observational ensemble in terms of their constraints on the distribution, speciation, and  
68 sources of VOC-carbon and reactivity, 2) assess our current scientific ability to capture that distribution  
69 across diverse environments, and 3) identify priorities for future research and model improvements.

70 It is widely recognized that terrestrial ecosystems provide the largest source of VOCs to the global  
71 atmosphere, mainly through foliar emissions but also via microbial decomposition of organic material,  
72 with an estimated flux of 750-1000 Tg/yr (Safieddine et al., 2017; Guenther et al., 2012). Global  
73 anthropogenic VOC emissions are thought to be an order of magnitude lower (e.g., 100-160 Tg/yr  
74 (Glasius and Goldstein, 2016; Boucher et al., 2013)), and include contributions from mobile sources such  
75 as on-road vehicles and aircraft (Stettler et al., 2011; Parrish, 2006) and from stationary sources such as  
76 volatile chemical products, fuel production, distribution, and combustion, and waste treatment (McDonald  
77 et al., 2018; Warneke et al., 2014; de Gouw et al., 2012; Millet et al., 2012). Biomass burning, i.e.,  
78 combustion of any non-fossilized vegetation, leads to an estimated 60-400 Tg/yr of emitted VOCs,  
79 though with high uncertainty regarding potential unidentified and/or unmeasured pyrogenic compounds  
80 (Giglio et al., 2013; Akagi et al., 2011; Wiedinmyer et al., 2011; Andreae and Merlet, 2001). Ocean-  
81 atmosphere VOC fluxes have been investigated with a range of aircraft- and ship-based observations,  
82 remote sensing, and modeling approaches for species including isoprene and monoterpenes, other light  
83 hydrocarbons, halogenated species, and oxygenated VOCs such as methanol, acetone, formaldehyde,  
84 acetaldehyde, glyoxal, and carboxylic acids (Deventer et al., 2018; Kim et al., 2017; Mungall et al., 2017;  
85 Coburn et al., 2014; Yang et al., 2014a; Yang et al., 2014b; Beale et al., 2013; Yang et al., 2013; Fischer  
86 et al., 2012; Beale et al., 2011; Luo and Yu, 2010; Millet et al., 2010; Shaw et al., 2010; Millet et al.,  
87 2008; Read et al., 2008; Palmer and Shaw, 2005; Williams et al., 2004; Singh et al., 2003; Broadgate et  
88 al., 1997; Zhou and Mopper, 1997; Bonsang et al., 1988; Kanakidou et al., 1988). However, the



89 quantitative role of the ocean as a net global VOC source or sink remains uncertain (Carpenter et al.,  
90 2012; Read et al., 2012).

91 While there have been a large number of studies focusing on one or a small subset of VOCs (a recent  
92 Web of Science search for articles with topic terms (“volatile organic compound\*”) AND (“atmospher\*”)  
93 returned >6,800 results), there have been few integrated studies examining the overall suite of measured  
94 species and our ability to capture that ensemble behavior in current CTMs. In one example, de Gouw et  
95 al. (2005) examined the photochemical evolution of organic carbon from urban outflow in the  
96 northeastern US and found evidence for unidentified aerosol precursors. Later, Goldstein and Galbally  
97 (2007) compiled a rough estimate of the total VOC budget and argued that there is a large pool of  
98 uncharacterized organic compounds in the atmosphere. Heald et al. (2008) carried out an integrated  
99 assessment of total observed organic carbon based on available measurements to that point, and  
100 articulated a need for more routine and comprehensive VOC-carbon measurements, while Safieddine et  
101 al. (2017) recently performed the first CTM-based budget analysis of total organic carbon on a global  
102 scale.

103 Recent observational work has benefited from new tools (e.g., high-resolution time-of-flight mass  
104 spectrometry) that enable a more thorough and time-resolved characterization of VOC-carbon than was  
105 previously possible. For instance, new flux measurements have been able for the first time to characterize  
106 the two-way surface atmosphere exchange of VOC-carbon simultaneously across the entire mass  
107 spectrum (Karl et al., 2018; Millet et al., 2018; Park et al., 2013). In addition, recent studies (Isaacman-  
108 VanWertz et al., 2018; Hunter et al., 2017) combining a comprehensive suite of online instrumentation  
109 have been able to achieve organic carbon closure (to within error) in a forested environment and in a  
110 laboratory oxidation experiment, respectively.

111 The past decade has thus seen major advances in the scientific community’s ability to measure (e.g.,  
112 Glasius and Goldstein (2016)) as well as model (e.g., Safieddine et al. (2017)) atmospheric organic  
113 carbon, and in our laboratory-derived understanding of key VOC oxidation pathways (e.g., (Praske et al.,  
114 2018; Ehn et al., 2014; Crouse et al., 2013; Paulot et al., 2009b)). Over the same period, there have been  
115 a large number of airborne campaigns over North America that, together, are unprecedented in their  
116 chemical and spatial coverage for characterizing VOC distributions over this region. Here, we perform an  
117 integrated analysis of these airborne datasets based on a high-resolution chemical transport model (nested  
118 GEOS-Chem CTM). The model simulation includes extensive new developments related to atmospheric  
119 VOCs and provides a more comprehensive representation of atmospheric organics than has been available  
120 for prior model-measurement evaluations. We apply this updated model with the suite of airborne  
121 observations to assess present understanding of the processes driving atmospheric VOCs, identify  
122 knowledge gaps, and address priorities for future work. We focus in this paper specifically on non-  
123 methane VOCs; we exclude intermediate, semi-volatile, low-volatility, and extremely low-volatility  
124 organic compounds (IVOC, SVOC, LVOC, ELVOC) because a comparable suite of airborne  
125 observations does not exist for these. The Hunter et al. study referenced above found for a ponderosa pine  
126 forest that while S/IVOC and E/LVOC species accounted for most of the aerosol-forming material, VOCs  
127 dominated the ambient OH reactivity due to non-methane organics, and also provided the majority of the  
128 organic carbon mass (Hunter et al., 2017). Likewise, while organic aerosol formation and subsequent  
129 deposition is not counted explicitly as a VOC sink in our chemical mechanism, prior work has found this  
130 to be only a small fraction (<4%) of the gas-phase VOC budget (Safieddine et al., 2017).

131



## 132 2. Model description

133 We use the GEOS-Chem CTM (v10-01; [www.geos-chem.org](http://www.geos-chem.org)) driven by assimilated meteorological  
134 fields (Goddard Earth Observation System Forward Processing product, GEOS-FP) from the NASA  
135 Goddard Modeling and Assimilation Office (GMAO). Simulations are performed for 2013, the year in  
136 which several of the utilized aircraft campaigns took place. The GEOS-FP fields have spatial resolution of  
137  $0.25^\circ \times 0.3125^\circ$  and temporal resolution of 3-h for 3-D meteorological parameters and 1-h for surface  
138 quantities and mixing depths. The North American simulation used here is conducted within a nested  
139 framework ( $130\text{--}60^\circ\text{W}$ ,  $9.75\text{--}60^\circ\text{N}$ , 47 vertical layers) at the native GEOS-FP horizontal resolution (Kim  
140 et al., 2015), with timesteps of 5-min (transport/convection) and 10-min (emissions/chemistry) (Philip et  
141 al., 2016). Dynamic boundary conditions are obtained from a global simulation ( $4^\circ \times 5^\circ$ ) with timesteps of  
142 30-min (transport/convection) and 60-min (emissions/chemistry). We use the TPCORE advection  
143 algorithm (Lin and Rood, 1996), convective mass fluxes from the GEOS-FP archive (Wu et al., 2007),  
144 and the non-local boundary layer mixing scheme described by Lin and McElroy (2010).

145 A year-long nested model run for 2013 was obtained via 12 parallel month-long simulations. Each of the  
146 latter was initialized after a ~1-week nested spin-up of regridded concentration fields from a ~2-year  
147 global spin-up. We find that this procedure is sufficient to achieve dynamic steady-state for oxidant and  
148 VOC levels in the model, as species that would require longer spin-up (e.g., methane) are prescribed  
149 rather than actively simulated in this mechanism.

### 150 2.1 Chemistry

151 The chemical mechanism in this work is based on Millet et al. (2018), with the following modifications.  
152 Here we incorporate a more detailed treatment of monoterpene chemistry that is adapted from Fisher et al.  
153 (2016), along with updated photo-isomerization yields for acetaldehyde (Millet et al., 2015). Further  
154 updates are included for VOC ozonolysis (isoprene, methacrolein, and isoprene hydroxynitrate) (Marais  
155 et al., 2016), glyoxal and methyl glyoxal yields from aromatics (Fischer et al., 2014), carboxylic acid  
156 production from the hydrolysis of stabilized Criegee intermediates (Millet et al., 2015), and photolysis  
157 cross sections for methyl vinyl ketone (MVK) and methacrolein (MACR) nitrates and propanone nitrate  
158 (Paulot et al., 2009a). Finally, we apply the carbon mass tracking approach outlined in Safieddine et al.  
159 (2017) to ensure carbon closure.

### 160 2.2 Deposition

161 Physical VOC sinks in GEOS-Chem include dry deposition following the Wesely (1989) scheme as  
162 implemented by Wang et al. (1998), and wet deposition as described by Amos et al. (2012). Wet  
163 deposition assumes liquid-phase-only uptake of VOCs (except formic acid and acetic acid) with a  
164 retention efficiency of 1 in warm clouds and 0.02 in mixed clouds (Mari et al., 2000). Ice uptake of  
165 formic acid and acetic acid is included based on the Langmuir isotherm model (Paulot et al., 2011).

166 Henry's law solubility constants ( $H$  values; required for calculating dry deposition resistances, gas-phase  
167 wet deposition, and air-sea fluxes) are computed following Travis et al. (2016) and Nguyen et al. (2015)  
168 for nitric acid, hydrogen peroxide, and a suite of isoprene-derived oxygenated VOCs (isoprene hydroxyl  
169 hydroperoxides, isoprene hydroxynitrate, isoprene epoxides, MVK/MACR nitrates, propanone nitrate,  
170 glycolaldehyde, hydroxyacetone). Values for lumped  $\geq\text{C}_4$  alkyl nitrates and formaldehyde are based on  
171 Marais et al. (2016) and Jacob (2000), respectively, while those for benzene, toluene, and xylene  
172 (representing lumped C8 aromatics) are taken from Staudinger and Roberts (2001). The lumped xylene  
173 species in the model uses the mean  $H$  value from the corresponding individual C8 compounds (o-xylene,  
174 m-xylene, p-xylene, ethylbenzene). For other VOCs we use central literature values based on the Sander  
175 (2015) compilation. Carboxylic acids employ an effective  $H$  value at  $\text{pH}=7$ , with lumped  $\geq\text{C}_3$  acids using  
176 the median reported value for propionic acid (Nirmalakhandan and Speece, 1988).



177 2.3 Emissions

178 2.3.1 Natural emissions

179 Biogenic VOC emissions from terrestrial plants are calculated online in GEOS-Chem using the Model of  
180 Emissions of Gases and Aerosols from Nature version 2.1 (MEGAN v2.1), implemented into GEOS-  
181 Chem as described by Hu et al. (2015) with updated  $0.25^{\circ} \times 0.3125^{\circ}$  distributions of plant functional types  
182 and base emission factors.

183  $\text{NO}_x$  emissions from microbial processes in soils are estimated as described in Hudman et al. (2012). The  
184 annual combined global flux of formic and acetic acids from soils estimated previously by Paulot et al.  
185 (2011) corresponds to approximately 10% of this  $\text{NO}_x$  source, and we therefore determine the  
186 formic/acetic acids soil fluxes as 5% (molar ratio) of the Hudman et al. (2012)  $\text{NO}_x$  flux.

187 Marine hydrocarbon emissions (for alkanes, alkenes, and isoprene) are estimated following Millet et al.  
188 (2015) and Paulot et al. (2011). Air-sea fluxes of oxygenated VOCs are calculated following Johnson  
189 (2010), Millet et al. (2010; 2008), and Fischer et al. (2012), with assumed fixed seawater concentrations  
190 of 15nM (acetone), 31nM (methanol), and 6nM (acetaldehyde) based on compiled cruise measurements  
191 (Beale et al., 2015; Yang et al., 2014a; Yang et al., 2014b; Beale et al., 2013; Yang et al., 2013; Beale et  
192 al., 2011; Kameyama et al., 2009; Hudson et al., 2007; Marandino et al., 2005; Williams et al., 2004;  
193 Zhou and Mopper, 1997).

194 2.3.2 Anthropogenic emissions

195 Global anthropogenic VOC emissions in the model are from the Interpolated ACCMIP-RCP 8.5  
196 inventory for year-2013 (van Vuuren et al., 2011; Lamarque et al., 2010; Riahi et al., 2007) (with a few  
197 exceptions; see below). This inventory provides speciated emissions for  
198 alkanes/alkenes/alkynes/aromatics, and unspciated emissions for alcohols/ $\geq\text{C}2$   
199 aldehydes/ketones/carboxylic acids. For the latter, we apply speciation factors for methanol and ethanol  
200 (0.5, 0.375, mass basis), acetaldehyde and  $\geq\text{C}3$  aldehydes (0.75, 0.25), and acetone and  $\geq\text{C}4$  ketones  
201 (0.75, 0.25) based on prior studies (Wells et al., 2012; Millet et al., 2010). Formic acid and acetic acid  
202 together are assumed to account for 75% by mass of the total ACCMIP carboxylic acid source (these in  
203 turn are partitioned with a 1:2 molar ratio), with  $\geq\text{C}3$  carboxylic acids making up the remaining 25%  
204 (Paulot et al., 2011).

205 Global anthropogenic and biofuel emissions of ethane and propane are from Xiao et al. (2008). Global  
206 formic and acetic acid emissions from animal agriculture are scaled to the corresponding ammonia source  
207 (from EDGAR v4.2 agricultural sectors 4C and 4D) following Paulot et al. (2011). We use global biofuel  
208 emissions from Yevich and Logan (2003) for emitted oxygenated VOCs not included in ACCMIP-RCP  
209 8.5 (glycolaldehyde, hydroxyl acetone, glyoxal, and methyl glyoxal). Aircraft emissions are from the  
210 AEIC inventory (Stettler et al., 2011), and global anthropogenic  $\text{NO}_x/\text{CO}/\text{SO}_2/\text{NH}_3$  emissions are from  
211 EDGAR v4.2 (European Commission (EC), 2011).

212 Over North America, emissions of inorganic species and VOCs (except ethane and propane) from  
213 anthropogenic, biofuel, and ship sources are overwritten by the hourly EPA/NEI2011 inventory (Travis et  
214 al., 2016; EPA, 2015), with annual scale factors applied to account for recent trends (e.g., the nationally  
215 aggregated 2011-2013 emission trend factor for VOCs is 0.971). Molar fluxes of formic and acetic acid  
216 over North America from these sources are estimated by scaling those of CO by  $2.1 \times 10^{-4}$  and  $4.2 \times 10^{-4}$ ,  
217 respectively (Paulot et al., 2011).

218 2.3.3 Biomass burning emissions

219 Open fire emissions are calculated from monthly burned area and fractional fire type contributions from  
220 the fourth version of the Global Fire Emissions Database with small fires (GFED4s) (van der Werf et al.,



221 2017) for our simulation year. We use the GFED-recommended species-specific emission factors  
222 (<http://www.globalfiredata.org/data.html>) which are based primarily on Akagi et al. (2011).

223

### 224 3. Airborne measurements of VOCs over North America

225 Figure 1 shows flight tracks for the airborne tropospheric chemistry missions that took place over North  
226 America between 2010-2014 and are used here. We have used data from intensive field campaigns using  
227 NCAR, NOAA and NASA aircraft that carried a large instrument payload to simultaneously measure  
228 many VOCs. Together, they provide a rich dataset for constraining VOC-related processes, as they  
229 feature extensive horizontal and vertical sampling throughout the North American troposphere and  
230 include a range of observing strategies such as survey transects, racetrack gradients/walls, and spirals.  
231 Table 1 summarizes the campaigns in terms of sampling time period, region, as well as aircraft platform  
232 and flight ceiling, with instrumental measurement details and references provided in Table S1. Below, we  
233 briefly introduce the overall goals and instrument payload for each campaign.

234 The Studies of Emissions and Atmospheric Composition, Clouds, and Climate Coupling by Regional  
235 Surveys (SEAC<sup>4</sup>RS 2013; Aug-Sep 2013) (Toon et al., 2016; SEAC<sup>4</sup>RS Science Team, 2013) was  
236 conducted over the southeastern US and targeted a broad range of goals including quantifying the  
237 regional distribution of anthropogenic, biomass burning, and biogenic chemicals, characterizing their re-  
238 distribution through convection, and identifying their impacts on boundary layer and upper tropospheric  
239 chemistry. The deployed NASA DC-8 aircraft has a flight ceiling of 12.5 km above sea level (ASL),  
240 enabling deep vertical profiling. The SEAC<sup>4</sup>RS VOC payload included a chemical ionization mass  
241 spectrometer using CF<sub>3</sub>O<sup>+</sup> reagent ions (CIT-CIMS (CF<sub>3</sub>O<sup>+</sup>)), a separate CIMS measuring peroxy acetyl  
242 nitrate (PAN-CIMS), a proton-transfer-reaction mass spectrometer (PTR-MS), in situ airborne  
243 formaldehyde measurements by laser induced fluorescence (ISAF-LIF), thermal dissociation LIF (TD-  
244 LIF), and a whole air sampler (WAS). Specific VOCs measured by each instrument are listed in Table S1.

245 The Southeast Nexus (SENEX; Jun 2013) campaign (Warneke et al., 2016) was part of the Southeast  
246 Atmosphere Study (SAS). The NOAA WP-3D aircraft sampled the boundary layer through mid-  
247 troposphere (up to 6.4 km ASL), targeting both natural and anthropogenic emissions. Onboard VOC  
248 instruments included WAS, ISAF-LIF, PAN-CIMS, and PTR-MS. SENEX also featured in-situ  
249 measurements of carboxylic acids by two separate CIMS using iodide reagent ions (I-CIMS) and of  
250 glyoxal via airborne cavity enhanced spectrometer (ACES) (Table S1).

251 The Deep Convective Clouds and Chemistry (DC3; May-Jun 2012) field experiments took place over the  
252 central US and were specifically designed to investigate changes in upper tropospheric composition and  
253 chemistry during and after deep convective events (Barth et al., 2015; DC3 Science Team, 2013). During  
254 DC3 the NASA DC-8 and GV aircraft sampled storm outflow up to 13 km ASL through spirals and wall  
255 sampling. The VOC payload included PTR-MS, a Trace Organic Gas Analyzer (TOGA), CIT-CIMS  
256 (CF<sub>3</sub>O<sup>+</sup>), PAN-CIMS, ISAF-LIF, TD-LIF, and WAS.

257 The California Research at the Nexus of Air Quality and Climate Change (CalNex; May-June 2010)  
258 campaign studied air quality and climate over California and offshore (Ryerson et al., 2013). The NOAA  
259 WP-3D aircraft sampled the troposphere up to 5 km ASL, and carried out survey tracks over the northern,  
260 central, and southern San Joaquin Valley and Los Angeles basin, with spirals over targeted urban and  
261 agricultural sources. VOCs were measured onboard by PTR-MS, PAN-CIMS, and WAS.

262 DISCOVER-AQ (Deriving Information on Surface Conditions from Column and Vertically Resolved  
263 Observations Relevant to Air Quality) (Crawford and Pickering, 2014; DISCOVER-AQ Science Team,



264 2014) included four separate airborne campaigns: DISCOVER-AQ DC (Jun-Jul 2011) over Baltimore-  
265 Washington DC, DISCOVER-AQ CA (Jan-Feb 2013) over the San Joaquin Valley, DISCOVER-AQ TX  
266 (Sep 2013) over Houston, and DISCOVER-AQ CO (Jul-Aug 2014) over the Denver Colorado urban  
267 region. The NASA P3-B aircraft (8.5 km ASL ceiling) was employed in each case, with frequent and  
268 repeated spirals to characterize the vertical structure of the troposphere. The VOC payload included a  
269 difference frequency generation absorption spectrometer (DFGAS) and time-of-flight PTR-MS (PTR-  
270 ToF-MS; quadrupole PTR-MS was used for DISCOVER-AQ DC).

271 FRAPPÉ (Front Range Air Pollution and Photochemistry Experiment; Jul-Aug 2014) took place jointly  
272 with DISCOVER-AQ CO, with the employed NCAR C-130 aircraft (8 km ASL ceiling) sampling the  
273 broader mountain-plain areas over northern Colorado. The VOC payload included PTR-MS, a compact  
274 atmospheric multi-species spectrometer (CAMS), TOGA, peroxide CIMS (PCIMS), PAN-CIMS, and  
275 WAS.

276 We use 1-minute merged data from each campaign to match the frequency at which the GEOS-Chem  
277 output is sampled along the aircraft flight tracks. For species co-measured by multiple instruments during  
278 the same campaign, we select one measurement primarily based on time response ( $\leq$  1-min sampling rate  
279 preferred), while also considering data availability and nominal accuracy. For example, VOCs measured  
280 by PTR-MS, TOGA or CAMS (for ethane) take precedence over contemporaneous WAS observations  
281 due to the higher time resolution. The ISAF-LIF, DFGAS and CAMS instruments are specifically  
282 designed for formaldehyde, and we use these observations (rather than WAS, TOGA, or PTR-MS) in all  
283 cases with the exception of CalNex (where PTR-MS was the only available HCHO measurement). PTR-  
284 MS and TOGA measurements during FRAPPÉ are highly correlated but with 5-30% discrepancies across  
285 compounds (Fig. S18). We therefore repeated our main analyses using data from each instrument (see  
286 Fig. 5, 6 and Table S2, S3), and find that the conclusions are not significantly changed. Similar sensitivity  
287 tests are done for formaldehyde, which had concurrent observations during DC3-DC-8 (DFGAS, ISAF-  
288 LIF) and during SEAC<sup>4</sup>RS (CAMS, ISAF-LIF), as well as for formic acid, which had concurrent  
289 observations during SENEX (NOAA CIMS, UW CIMS) (Fig. S19).

290 One concern when combining multiple measurements is the differing time resolution between  
291 instruments. For example, the WAS systems collect discrete samples separated by up to 10 min, while  
292 TOGA collects a 35 second integrated sample on alternate minutes. Many other instruments used here  
293 have significantly higher time resolution. To address this issue, when mapping aggregated quantities (i.e.,  
294 total VOC-carbon; Fig. 5), we consider only those datapoints with complete species coverage (no missing  
295 data within a given campaign's payload). Overall, this yields ~7000 (4500) 1-min averaged observational  
296 datapoints in the PBL (FT), distributed over ~900 (1700) ~25km model grid cells. Finally, to avoid  
297 comparing a single modeled value with multiple observations falling into the same model gridbox and  
298 timestep, all measurements and model output are averaged and gridded to unique model gridbox-timestep  
299 combinations.

300

#### 301 4. Simulated VOC budget over North America

##### 302 4.1 Biogenic emissions dominate the VOC budget on a carbon basis

303 Figure 2a depicts the annual VOC budget (in C units) over North America in 2013 as simulated by  
304 GEOS-Chem. A buffer of ten model grid boxes along each lateral boundary has been omitted to exclude  
305 unrealistic conditions near the edge of the nested domain. Total fluxes are indicated for each source and  
306 sink term, representing the sum over all grid boxes within the plotted region. The net transport flux in/out  
307 of the domain is estimated from the accumulated product of the daily average eastward/northward wind



308 components and VOC number density at the boundaries. In this way, we achieve regional VOC-carbon  
309 closure to within 3%.

310 We see in Fig. 2a that biogenic emissions are the dominant annual VOC-carbon source over North  
311 America, accounting for 71% (40 TgC) of the model total. Anthropogenic emissions account for 23% (13  
312 TgC), while VOC emissions from fires can be important in particular locations and seasons but are minor  
313 when integrated over the domain as a whole (3 TgC, 5%). Prior studies have estimated that biogenic VOC  
314 emissions are 10-12× larger than anthropogenic emissions on a global basis (Safieddine et al., 2017;  
315 Glasius and Goldstein, 2016; Boucher et al., 2013; Guenther et al., 2012; Goldstein and Galbally, 2007);  
316 our results for North America, while indicating a greater relative importance for anthropogenic emissions  
317 than in the global mean, still show that biogenic VOC-carbon emissions are ~3× anthropogenic sources  
318 even in this industrialized region. Finally, while methane is not considered as a VOC for the purpose of  
319 our analysis, its oxidation generates formaldehyde and methyl hydroperoxide, corresponding to a VOC  
320 source of 30 TgC/y over our North American domain. Methane oxidation is thus >2× larger as a non-  
321 methane VOC source over this region than anthropogenic emissions, though this source is diffuse and  
322 not-collocated with land-based fluxes.

323 During winter (Fig. 3a), we find in the model that anthropogenic sources account for the majority (54%)  
324 of emitted VOC-carbon over the domain as a whole; this fraction would be significantly higher if we were  
325 to exclude the US Gulf States, Mexico, and Central America where substantial biogenic emissions persist  
326 throughout the year. However, during summer the modeled domain-wide anthropogenic contribution is  
327 only 12%; then, it is only in the most polluted regions, where biogenic emissions are low, that  
328 anthropogenic emissions provide the main source of atmospheric reactive carbon.

#### 329 4.2 Biogenic VOC emissions even more dominant on a reactivity basis

330 The predominance of biogenic over anthropogenic VOCs in North America is even more pronounced  
331 when we account for the chemical reactivity of the various species. A common metric for assessing this is  
332 the OH reactivity ( $\sum k_i n_i$ , where  $k_i$  and  $n_i$  are the OH reaction rate coefficient and atmospheric number  
333 density for chemical  $i$ ), which quantifies the OH loss rate associated with the ambient loadings of various  
334 species. In this paper, we use the term ‘VOC reactivity’ to refer specifically to that portion of the OH  
335 reactivity driven by VOCs. A related, emissions-focused measure is the OH reactivity flux: i.e.,  $\sum k_i F_i$ ,  
336 where  $F_i$  is the surface flux for VOC  $i$  (in molecular units). Since the reactivity flux is equivalent to a  
337 (mixing-height scaled) time-derivative of OH reactivity (Millet et al., 2018), it provides a direct measure  
338 of how a given surface flux affects ambient OH reactivity.

339 Figure 2b maps the modeled OH reactivity flux associated with biogenic, anthropogenic and pyrogenic  
340 VOC emissions. We see that biogenic sources in the model account for 95% of the annual reactivity-  
341 weighted VOC source over North America as a whole, with anthropogenic sources contributing just 3%.  
342 This biogenic predominance continues throughout the year, with biogenic VOCs making up 88% of the  
343 modeled domain-aggregated reactivity flux even during winter (though with strong spatial gradients; Fig.  
344 3b). During summer, that fraction increases to 96%.

345 There has been a substantial decrease in transportation-related VOC emissions over the past several  
346 decades in the US (McDonald et al., 2013; Parrish, 2006) (e.g., a factor of ~50-100 decrease was inferred  
347 over Los Angeles from 1960-2010 (Warneke et al., 2012)). According to current inventories (Fig. 3),  
348 anthropogenic emissions have declined to the point where biogenic emissions are the dominant  
349 summertime source of VOC reactivity even in many major North American cities. Only in a small  
350 number of pollution hotspots (Fig. 3) are anthropogenic emissions the main source of VOC-related OH  
351 reactivity driving summertime production of ozone and other secondary products.





352 4.3 Anthropogenic species comprise over half of the ambient VOC-carbon burden over most of North  
353 America

354 Figure 4 (panels b, c, e, and f) shows the fractional contribution to the ambient near-surface VOC burden  
355 from anthropogenic and biogenic emissions. We quantify these contributions via model sensitivity tests  
356 with modified (-10%) biogenic and anthropogenic VOC emissions; the contribution from each emission  
357 category is then obtained by dividing the relative change in ambient VOC-carbon or reactivity by the  
358 relative emission perturbation. Partitioning the ambient VOC loading in this way provides an alternate  
359 framing of the VOC budget compared to the discussion above, which examined the VOC source flux  
360 magnitudes themselves.

361 While anthropogenic species make up only a small fraction of the total emitted VOC mass (~23%; Fig.  
362 1), they account for more than half of the ambient near-surface VOC-carbon abundance over most of the  
363 North American domain (the median fraction in Fig. 4c is 57%). This is due to the longer aggregate  
364 model lifetime for anthropogenic versus biogenic VOCs: because of this, away from major biogenic  
365 source regions the ambient VOC-carbon loading predominantly reflects anthropogenic species. However,  
366 many of these areas have relatively low total VOC-carbon loading (Fig. 4a). The corollary of the above  
367 finding is that the ambient VOC-driven OH reactivity is controlled by biogenic species, and this is also  
368 apparent in Fig. 4 (panels e and f).

369 4.4 Fate of reactive carbon over North America

370 The predominance of biogenic VOCs (in terms of total emitted VOC-carbon) combined with their  
371 relatively short ensemble lifetime leads to a spatial correlation between biogenic VOC emissions and total  
372 VOC sinks (e.g., over the southeastern US; Fig. 2a). Fig. 2a shows that of the 86 TgC of non-methane  
373 VOC added annually to the North American atmosphere through emissions, transport, and CH<sub>4</sub> oxidation,  
374 62 TgC (72%) is oxidized to CO+CO<sub>2</sub> in the model. If we exclude the oxidation of methane (nearly 100%  
375 of which goes on to form CO and CO<sub>2</sub>), then of the 56 TgC/y of primary VOCs emitted over North  
376 America, 32 TgC/y (57%) is ultimately oxidized to CO+CO<sub>2</sub> within the domain of Fig. 2. Oxidation of  
377 non-methane VOCs therefore provides an atmospheric CO+CO<sub>2</sub> source over this region slightly larger  
378 than that from methane oxidation.

379 Other removal processes include deposition (dry, 10 TgC/y; wet, 7 TgC/y) and net transport out of the  
380 domain (10 TgC/y). While global studies have found that wet deposition is a ~50% larger sink of organic  
381 carbon than is dry deposition (Safieddine et al., 2017; Kanakidou et al., 2012), the increased role for dry  
382 deposition found here is consistent with the higher continental coverage of our regional domain.

383 In the case of the VOC reactivity budget (Fig. 2b), we find in GEOS-Chem that chemical degradation is  
384 by far the largest sink (83%) of emitted reactivity, with physical removal via deposition (14%) and  
385 transport out of the domain (3%) making up the remainder.

386

### 387 **5. Observed versus predicted distribution of VOC-carbon and reactivity over North America**

388 In this section we use the aircraft campaigns described earlier to characterize the distribution of VOCs  
389 over North America, and assess the ability of the GEOS-Chem model to capture that distribution in terms  
390 of total carbon loading and associated reactivity.

391 For each campaign we use the 1-minute merge products provided by the NASA Langley Research Center  
392 (LaRC) and the NOAA Earth System Research Laboratory Chemical Science Division (ESRL CSD)  
393 (Table 1), and sample the model along the flight tracks at the time of measurement. Measurements have  
394 been filtered to remove fresh biomass burning (CH<sub>3</sub>CN > 0.2 ppbv) and pollution plumes (NO<sub>2</sub> > 4 ppbv)



395 or  $\text{NO}_x/\text{NO}_y > 0.4$ ), and restricted to daytime measurements over continental North America. Model-  
396 measurement comparisons are performed for the planetary boundary layer (PBL, defined here as  $< 2$  km  
397 AGL) and free troposphere (FT,  $> 3$  km AGL) based on unique gridbox-timestep combinations.

398 For the purposes of model-measurement comparison we restrict the observed VOCs to those that are  
399 explicitly simulated by GEOS-Chem (Millet et al., 2018). This restricted set of VOCs nonetheless  
400 encompasses those species believed to be most important in terms of abundance and reactivity (Heald et  
401 al., 2008), and allows an apples-to-apples comparison between observations and model. For cases where  
402 multiple VOCs are measured together as a single quantity, the corresponding modeled VOCs are likewise  
403 summed. Similarly, measured VOCs are summed to match those that are lumped in the model.

404 VOC OH reactivities are calculated from the measured and simulated species concentrations and  
405 corresponding pressure- and temperature-dependent rate coefficients for reaction with OH. For species  
406 that are detected together but simulated separately, we use the modeled ratio to partition the measured  
407 sum in calculating the combined OH reactivity. For species that are lumped in the model but measured  
408 separately, we apply the bulk OH reaction rate coefficient from the model to the summed measurements.

409 In the case of C3 and C4 ketones and aldehydes, the model includes a dedicated tracer for acetone  
410 (ACET) and lumped tracers for  $\geq \text{C4}$  ketones (MEK) and  $\geq \text{C3}$  aldehydes (RCHO). On the other hand,  
411 these species are measured by PTR-MS as  $\Sigma(\text{acetone} + \text{propanal})$  and  $\Sigma(\text{MEK} + \text{butanal})$  and by TOGA as  
412 individual species. When analyzing the PTR-MS data we therefore partition the PTR-MS observations  
413 based on the median aldehyde:ketone ratio measured by TOGA during FRAPPÉ and DC3 (0.009 for  
414 propanal:acetone and 0.09 for butanal:MEK).

#### 415 5.1 Total observed VOC-carbon and reactivity over North America

416 Figure 5 (left panels) shows the resulting total VOC-carbon as observed over North America, which  
417 averages 27 ppbC in the PBL when considering all the aircraft campaigns as a single statistical ensemble.  
418 However, the campaigns span a range of instrumental payloads, seasons, and locations: campaigns with  
419 the most comprehensive VOC instrument payloads and that occur during summer reveal total PBL VOC  
420 loadings generally  $> 60$  ppbC, and up to 133 ppbC over the central and southeastern US. Campaigns over  
421 the northeastern and western US, with more limited VOC payloads, show PBL VOC loadings that  
422 average 20 ppbC and at times exceed 50 ppbC. Total VOC loadings in the FT (Fig 5a) drop by a factor of  
423  $\sim 3$  or more from those in the PBL across all environments, with an ensemble spatial mean of 9 ppbC.

424 The observed VOC-carbon loadings summarized above and plotted in Fig. 5 are broadly similar to those  
425 reported over the US by Heald et al. (2008) (averaging 8-84 ppbC with 83-97% in the gas-phase at 273K  
426 and 1013hPa), who synthesized the gas- and aerosol- phase organic carbon observations up to that time.  
427 However, observations over the US used in that study were primarily from ground-based campaigns. The  
428 10 airborne studies carried out since then and used here allow a more comprehensive spatial description  
429 of VOCs across the North American airshed. The combined dataset employed here also includes a  
430 number of additional multifunctional VOCs that can now be quantified thanks to measurement advances  
431 in the intervening decade (Glasius and Goldstein, 2016).

432 Figure 6 (left panels) shows the total OH reactivity arising from the set of observed VOC. The aggregated  
433 spatial mean VOC reactivity is  $2 \text{ s}^{-1}$  in the PBL, declining to  $0.13 \text{ s}^{-1}$  in the FT. Compared to the VOC-  
434 carbon loading, the reactivity has a much larger vertical falloff (10-20 $\times$  decrease from the PBL to the FT),  
435 and greater spatial variability within the PBL. The observed VOC reactivity within the PBL is  
436 generally  $> 6 \text{ s}^{-1}$  over the southeastern US, 2-6  $\text{ s}^{-1}$  over the northeastern US, and  $< 2 \text{ s}^{-1}$  over the central and  
437 western US. The highest observed VOC reactivity ( $24 \text{ s}^{-1}$ ) over the southeastern US is comparable to



438 ground-based measurements in that region ( $10\text{-}25\text{ s}^{-1}$ ) during the SOAS study (Feiner et al., 2016; Kaiser  
439 et al., 2016).

440 The importance of biogenic VOCs for reactive carbon loading and, especially, reactivity in the PBL is  
441 evident in the maps shown in Fig. 5-6. For example, Fig. 6 shows sharply defined areas of elevated VOC  
442 reactivity in the PBL over the forests of the southeastern US, with strong horizontal gradients and much  
443 lower observed reactivity elsewhere. Similar patterns, though less starkly defined, are evident in the  
444 measured VOC-carbon distribution (Fig. 5). The highly reactive nature of many biogenic VOCs  
445 (especially isoprene and some of its oxidation products) explain their disproportionate impact on  
446 reactivity given their relative abundance, as well as the much larger spatial gradients for VOC reactivity  
447 than for total VOC-carbon.

#### 448 5.2 Speciated drivers of ambient VOC-carbon and reactivity

449 Figures 7 and 8 show the species driving ambient VOC-carbon and reactivity as a function of their carbon  
450 oxidation state ( $OS_c$ ) and size (carbon number,  $n_c$ ) (Kroll et al., 2011). Within the PBL (Fig. 7b), we find  
451 that the total mean VOC-carbon is largely driven by small and relatively reduced VOCs (e.g., acetone,  
452 methanol and alkanes), though some more oxidized species (e.g., formic acid, methyl hydroperoxide,  
453 formaldehyde, other isoprene oxidation products) also make significant contributions. These smaller  
454 VOCs would represent an even larger portion of the total molar VOC-loading.

455 In the FT (Fig. 7a), mean abundances decline by  $\sim 2$ -fold or more for all measured VOCs relative to the  
456 PBL. Here, a few small, reduced (low- $OS_c$ ), and relatively long-lived species dominate the overall VOC-  
457 carbon loading, with acetone, methanol, and ethane ( $\tau \sim 12\text{-}50$  days at  $OH = 10^6$  molecules/cm<sup>3</sup>) together  
458 averaging 6.4 ppbC, compared to only 3.6 ppbC for the mean sum of all other observed species.

459 However, ambient OH reactivity is driven by a different set of VOCs. Figure 8 shows that within the  
460 PBL, formaldehyde ( $0.34\text{ s}^{-1}$ ), acetaldehyde ( $0.19\text{ s}^{-1}$ ), isoprene hydroxyhydroperoxides + epoxides ( $0.21$   
461  $\text{s}^{-1}$ ), methylhydroperoxide ( $0.17\text{ s}^{-1}$ ), and isoprene ( $0.11\text{ s}^{-1}$ ) make the largest contributions to the mean  
462 observed VOC reactivity. Compared to the case for VOC-carbon loading (Fig. 7b), we see in the  
463 reactivity distribution a more prominent role for a number of higher- $n_c$  (and more reactive) compounds.

464 On average, the observed VOC reactivity is more than a factor of 10 lower in the FT than in the PBL,  
465 with formaldehyde ( $0.03\text{ s}^{-1}$ ) and acetaldehyde ( $0.02\text{ s}^{-1}$ ) still making the largest contributions to the total.  
466 Whereas the FT VOC-carbon loading is dominated by a few small VOCs (Fig. 7a), Figure 8a shows that  
467 the FT VOC reactivity is provided by a wider suite of species due to the offsetting effects of abundance  
468 and lifetime. In other words, we see important FT reactivity contributions (in the mean) from both highly-  
469 reactive (but low-abundance) VOCs such as isoprene, and from less-reactive (but highly-abundant) VOCs  
470 such as methanol.

#### 471 5.3 Accuracy of CTM-predicted VOC-carbon and reactivity

472 Figures 5 and 6 also portray the ability of the GEOS-Chem CTM to represent the measured distribution of  
473 VOCs over North America. In the PBL, the model exhibits significant skill at capturing atmospheric  
474 variability in VOC-carbon and reactivity: spatial model-measurement  $R^2$  values are 0.36 and 0.54,  
475 respectively. The same is not true in the FT, where the model-measurement correlations are  $R^2 < 0.1$  for  
476 both VOC-carbon and VOC OH reactivity. This lack of explanatory power suggests that the primary  
477 drivers of VOC abundance and reactivity in the FT are not well-understood or represented in current  
478 models.

479 We also see in Fig. 5 and 6 that the model tends to underestimate the observed VOC-carbon and reactivity  
480 in the PBL across most of the sampled environments, with a normalized mean bias (NMB) of -37% and -



481 34%, respectively. This corresponds to a mean reactive carbon underestimate in the PBL of 10 ppbC and  
482 a reactivity underestimate of  $0.6 \text{ s}^{-1}$ . A bias of this magnitude is equivalent to  $\sim 2\times$  the reactivity of  
483 methane (at 2ppm) or  $0.5\times$  that of CO (at 200 ppb), and is therefore important for accurately representing  
484 atmospheric OH chemistry and ozone production.

485 While on average the CTM underpredicts the abundance and reactivity of VOCs in the PBL, this is not  
486 the case everywhere. There are areas shown in Fig. 5 and 6 where the model either agrees with the  
487 observations or is too high - in particular over the northern Sacramento Valley and the southeastern US.  
488 Regarding the former, large methanol and acetaldehyde emissions from rice fields, with strong  
489 enhancements after flooding, were previously inferred based on the same CalNex observations over the  
490 Central Valley (Peischl et al., 2012; Warneke et al., 2011). Indeed, we find here a model overestimate of  
491 total VOC-carbon for this region before flooding and a low bias after flooding, suggesting that  
492 agricultural VOC emissions are not currently well-represented in the model. On the other hand, over the  
493 southeastern US, where biogenic emissions predominate and VOC loading is highest across all sampled  
494 areas, both the PBL VOC-carbon (observed mean of 48 ppbC) and VOC reactivity ( $4.5 \text{ s}^{-1}$ ) are captured  
495 by the model with low mean bias ( $<14\%$  for both).

496 In contrast to the PBL where both positive and negative model discrepancies occur, aloft in the FT the  
497 model exhibits a large negative bias for both VOC-carbon ( $-64\%$ ) and reactivity ( $-63\%$ ) that manifests  
498 essentially everywhere. Such a severe discrepancy has implications for our understanding of FT  $\text{HO}_x$   
499 cycling (Brune et al., 2018; Mao et al., 2009), ozone production at higher altitudes where its climatic  
500 effects are strongest (Apel et al., 2015; Bertram et al., 2007), and possibly, secondary organic aerosol  
501 loading (Bianchi et al., 2016; Cappa, 2016; Kirkby et al., 2016; Trostl et al., 2016; Heald et al., 2005). We  
502 explore potential causes for these observed discrepancies in Sec 6.1.

#### 503 5.4 Key VOCs driving model biases in atmospheric VOC-carbon and reactivity

504 Figure 7b shows that the overall low model bias for VOC-carbon in the PBL manifests for 23 out of 34  
505 individual VOCs, with these exhibiting normalized biases ranging from  $-1\%$  to  $-90\%$  (Fig. S1b and S2b).  
506 In general, the largest absolute carbon biases are seen for the more abundant VOCs (Fig. 7b), and largest  
507 reactivity biases for the more reactive VOCs (Fig. 8b). Just two compounds (acetone and methanol)  
508 account for almost half of the mean negative VOC-carbon bias seen in the PBL ( $4.3$  of  $9 \text{ ppbC}$ ). For  
509 VOC-reactivity, four compounds (methyl hydroperoxide, acetaldehyde, formaldehyde, and isoprene)  
510 together account for 70% of the mean model bias in the PBL ( $-0.34$  of  $-0.47 \text{ s}^{-1}$ ).

511 Aloft in the FT (Fig. 7a and 8a), we see appreciable relative biases manifest across nearly all model  
512 compounds (ranging from  $-7\%$  to  $-100\%$ ; Fig. S1a and S2a), with 29 of out of 34 VOCs biased low in the  
513 model by more than a factor of 2. Acetone, methanol, and ethane are predominant in driving the overall  
514 model VOC-carbon underestimate: these three species have a combined model bias of  $-3.3 \text{ ppbC}$ , versus a  
515 total of only  $-2.1 \text{ ppbC}$  for all other underestimated VOCs combined. Significant discrepancies in model  
516 simulated FT VOC-reactivity are driven by both abundant but less reactive VOCs, and by reactive (but  
517 less abundant) VOCs, with acetaldehyde having by far the largest absolute bias overall ( $-0.015 \text{ s}^{-1}$ ).

518 The above comparisons point to research priorities for improving current model representations of  
519 atmospheric VOCs. Along with highly abundant VOCs (such as acetone, methanol, and ethane),  
520 acetaldehyde, formaldehyde, isoprene (plus its oxidation products), and methyl hydroperoxide drive a  
521 large fraction of total VOC-reactivity and associated model biases. Advancing our current ability to  
522 model the sources, chemistry, and physical removal of this relatively small number of species could  
523 substantially improve predictions of VOC-carbon and reactivity distributions.

524



## 525 **6. Role of vertical transport in driving a persistent model VOC underestimate in the free** 526 **troposphere over North America**

527 In Sect. 5 we demonstrated that VOC abundance and reactivity are consistently underestimated by the  
528 model in the free troposphere across environments and compounds. Potential explanations for these  
529 missing FT VOCs include chemical effects (e.g., model biases in FT VOC production and loss rates) as  
530 well as dynamical effects (e.g., model biases in PBL-FT mixing). To help distinguish between these two,  
531 we plot in Fig. 9a the modeled versus observed mean PBL:FT ratio (mixing ratio units) for each VOC  
532 across the entire SEAC<sup>4</sup>RS campaign. We see that all data fall above the 1:1 ratio line, showing that the  
533 model is overestimating the PBL:FT ratio to a similar degree across all VOCs regardless of source,  
534 lifetime, and chemical properties. This consistency across compounds points to a misdiagnosis of PBL  
535 ventilation as a likely explanation for the persistent VOC underestimate in the FT (at least over the  
536 SEAC<sup>4</sup>RS domain), since other tenable mechanisms would not be expected to affect all VOCs in such a  
537 consistent way. In particular: i) a missing FT photochemical VOC source would not explain the PBL:FT  
538 discrepancy seen for primary VOCs; ii) a model bias in dry deposition or wet scavenging would  
539 differentially affect polar and soluble versus nonpolar and less soluble species; and iii) a model OH bias  
540 would impact reactive and longer-lived species to differing degrees. Findings similar to those shown in  
541 Fig. 9a are obtained for other campaigns over the southern and eastern US (SENEX, DISCOVER-AQ  
542 DC, DISCOVER-AQ TX) but not consistently elsewhere (DC3, DISCOVER-AQ CO, FRAPPÉ,  
543 DISCOVER-AQ CA, CalNex). Since the southeastern US is the major source of North American VOC-  
544 carbon and reactivity (Fig. 2), such a mixing bias would yield a significant model underestimate of the  
545 total amount of reactive organic carbon that is transported to the North American FT.

546 We can explore this issue further by considering a two-box model to conceptualize VOC partitioning  
547 between the PBL and FT. In that case, for an example VOC that is directly emitted and then subject to  
548 chemical loss by OH, PBL-FT mixing, and deposition (PBL only), the steady-state PBL:FT ratio would  
549 be linearly related to the OH rate coefficient  $k_{OH}$  with a slope determined by OH and by the PBL  
550 ventilation rate, and with an intercept determined by the PBL-FT mixing rates. Figure S3 shows that the  
551 same holds for secondary VOCs. While dilution with PBL and FT background air will also affect the  
552 PBL:FT ratio, its effect in this simplified framework will diminish as the extent of the domain considered  
553 increases, and for shorter-lived species.

554 Of the aircraft campaigns considered, SEAC<sup>4</sup>RS comes closest to the above approximation due to the  
555 larger spatial domain sampled by the DC8 aircraft. The modeled and observed PBL:FT ratios for this  
556 campaign are plotted in Fig. 9b as a function of  $k_{OH}$ . For both model and measurements, there is an  
557 approximately linear relationship, with the model generally capturing the observed PBL:FT vs.  $k_{OH}$  slope.  
558 However, with only a couple of exceptions (e.g., HCHO, C<sub>2</sub>H<sub>2</sub>), there is a clear offset between the two  
559 populations that manifests in a consistent way for both primary and secondary VOCs and across lifetimes.  
560 The offset persists even after correcting for a potential 40% PBL depth overestimate (Zhu et al., 2016) in  
561 the GEOS fields (Fig. S4). The same conclusions are obtained if we instead examine the PBL:(PBL+FT)  
562 or (PBL+FT):PBL ratios to minimize any potential influence from spurious ratios caused by near-  
563 detection-limit VOC measurements (not shown). Overall, the above comparisons implicates PBL:FT  
564 mixing as a likely player in the pervasive model VOC biases found in the FT.

565

## 566 **7. Role of biogenic versus anthropogenic sources in driving model biases for key oxygenated** 567 **VOCs in the North American boundary layer**

568 Section 5 demonstrated the critical role that certain light OVOCs (e.g., formaldehyde, acetaldehyde,  
569 methanol, acetone, methyl hydroperoxide) play in defining atmospheric VOC-carbon loading and



570 associated reactivity, and in driving model biases in those quantities. We see in Fig. 6 that while the  
571 GEOS-Chem model underestimates the abundance of most OVOCs in the PBL, some species are  
572 overestimated (analogous discrepancies are seen in the average vertical profiles; Fig. S5-14). We  
573 therefore investigate in this section the likely role of biogenic versus anthropogenic sources in driving the  
574 observed model biases for key OVOCs.

575 To this end, a unique pair of biogenic ( $\mathcal{B}_{OVOC}$ ) and anthropogenic ( $\mathcal{A}_{OVOC}$ ) source tracers was developed  
576 for each OVOC based on the mixing ratio difference along the flight track between the model base-case  
577 and simulations with either biogenic or anthropogenic emissions perturbed by 10%.  $\mathcal{B}_{OVOC}$  thus  
578 represents the integrated influence of direct biogenic emissions plus oxidation of biogenic precursors for a  
579 given OVOC along the aircraft flight track, based on the model simulation.  $\mathcal{A}_{OVOC}$  is likewise a marker  
580 for the combined influence of primary plus secondary anthropogenic sources. We find that the above  
581 tracers are best able to capture the observed in-PBL OVOC variance for the SEAC<sup>4</sup>RS, SENEX, and  
582 DISCOVER-AQ TX campaigns (Table S4), arguing that the allocation of model VOC sources has the  
583 highest spatial reliability over the southeastern US region. We therefore focus our source-tracer  
584 interpretation on these specific campaigns.

585 Figure 10 plots the model bias for select OVOCs as a function of  $\mathcal{B}_{OVOC}$  and  $\mathcal{A}_{OVOC}$ , and shows that in  
586 several cases the model OVOC errors exhibit a clear relationship with one (or both) of these source  
587 tracers. For example, the positive model bias seen previously (Fig. 6) for hydroxyacetone (HAC), methyl  
588 ethyl ketone (MEK), and glyoxal (CHOCHO) is strongly correlated with the biogenic source tracer  
589  $\mathcal{B}_{OVOC}$  for each species, with the largest model overestimates occurring when  $\mathcal{B}_{OVOC}$  is high. This points  
590 to a current model overestimate of the biogenic sources of HAC, MEK, and CHOCHO, either due to  
591 biases in their precursor emissions (e.g., (Kaiser et al., 2018; Zhu et al., 2016; Wolfe et al., 2015)) or in  
592 their chemical formation mechanisms (e.g., (Miller et al., 2017; Li et al., 2016)). Model sink errors may  
593 also play a role (e.g., (Curry et al., 2018)); however, to explain the results in Fig. 10, such biases would  
594 need to be spatially correlated with emissions.

595 Conversely, in the case of formic acid (HCOOH) the model bias becomes more negative with increasing  
596 biogenic influence (consistent results are obtained with either the UW or NOAA measurements, Fig.  
597 S16), which is consistent with earlier findings (Millet et al., 2015; Stavrou et al., 2012) pointing to an  
598 underestimated biogenic source of HCOOH or its precursors over the southeastern US. The negative  
599 model bias seen for PAA (Fig. 7) increases with both  $\mathcal{B}_{OVOC}$  and  $\mathcal{A}_{OVOC}$  (Fig. 10), which may indicate a  
600 generic underestimate of PAA production across biogenic and anthropogenic VOCs or an overestimation  
601 of its chemical loss.

602 Findings for other OVOCs tend to be less clear and/or less consistent across these campaigns.  
603 Acetaldehyde ( $\text{CH}_3\text{CHO}$ ) is biased low in the model, on average, across the aircraft campaigns (Fig. 7),  
604 and there is some indication that this is partly due to underrepresented anthropogenic sources (Fig. 10,  
605 S15-S17). Acetone and methanol are strongly underestimated by the model (Fig. 7), which drives a  
606 significant part of the overall model VOC-carbon bias over North America. However, Fig. 10 shows that  
607 while the model bias is negative under low values of  $\mathcal{B}_{OVOC}$ , it is positive under high values of  $\mathcal{B}_{OVOC}$   
608 (this is specifically the case for SEAC<sup>4</sup>RS and DISCOVER-AQ TX; Fig. S15-S17): this may indicate a  
609 model overestimate of direct biogenic emissions combined with an underestimate of regional background  
610 concentrations or of other sources.

611



## 612 8. Summary

613 We performed an integrated analysis of the atmospheric VOC budget over North America based on an  
614 ensemble of recent airborne observations interpreted with an updated version of the GEOS-Chem CTM.  
615 86 TgC of non-methane VOC is added annually to the North American atmosphere in the model through  
616 emissions (biogenic: 40 TgC; anthropogenic 13 TgC; fires: 3 TgC), and CH<sub>4</sub> oxidation (30 TgC/y). Of  
617 that, 62 TgC is oxidized to CO/CO<sub>2</sub>, with the rest removed by deposition (dry: 7 TgC/y; wet: 10 TgC/y)  
618 and net transport out of the domain (10 TgC/y).

619 The simulated North American VOC budget shows the dominance of biogenic VOC emissions on a  
620 carbon basis (71%) and even more markedly on a reactivity basis (95%). Anthropogenic emissions  
621 provide the dominant summertime source of VOC-carbon and reactivity only in a fairly small number of  
622 pollution hotspots, and annually is >2× smaller as a source of non-methane VOC over North America  
623 than is methane oxidation. Nevertheless, anthropogenic VOCs provide more than half of the ambient  
624 VOC-carbon burden over the majority of the region due to their longer average lifetime relative to  
625 biogenic species.

626 While on-road VOC emissions in North America have undergone a substantial decrease in the past few  
627 decades (McDonald et al., 2013; Warneke et al., 2012), recent studies have pointed to the importance of i)  
628 emerging VOC sources from oil and gas facilities (Li et al., 2017; Pfister et al., 2017), ii) volatile  
629 chemical products (McDonald et al., 2018), and iii) unexpectedly large urban OVOC fluxes (Karl et al.,  
630 2018). It is possible that such sources are not well captured in current inventories such as those used here,  
631 which in turn could alter the budget understanding above. These areas require further research to better  
632 understand the importance of such emissions for atmospheric chemistry, and to test and improve their  
633 representation in models.

634 Based on the collective aircraft observations, we find that total ambient VOC-carbon over North America  
635 is dominated by small and relatively reduced VOCs (e.g., acetone, methanol, alkanes), along with some  
636 oxidized species (e.g., formic acid, methyl hydroperoxide, formaldehyde, other isoprene oxidation  
637 products) that are also substantial VOC-carbon reservoirs in the planetary boundary layer (PBL). In the  
638 free troposphere (FT), acetone, methanol, and ethane together average 6 ppbC over the ensemble of  
639 airborne data, compared to only 4 ppbC for the sum of all other measured VOCs. Formaldehyde and  
640 acetaldehyde provide the largest source of VOC reactivity, on average, in both the PBL and FT, with a  
641 range of other reactive (but less abundant) and abundant (but less reactive) species also making  
642 significant contributions.

643 The GEOS-Chem CTM with state-of-science VOC treatment captures a significant portion of the  
644 observed ambient variability for VOC-carbon ( $R^2 = 0.36$ ) and reactivity (0.54) in the PBL, but not in the  
645 FT (0.07 and 0.04) – suggesting that the main factors influencing VOC abundances in the FT are  
646 inadequately represented in current models. The GEOS-Chem model exhibits both underestimates and  
647 overestimates of the observed VOC-carbon and reactivity in the PBL, depending on location, with an  
648 overall normalized mean bias of -37% (carbon) and -34% (reactivity). This mean bias is equivalent to ~2×  
649 the reactivity of methane at 2 ppm or 0.5× that of CO at 200 ppb, and is therefore important from the  
650 point of view of accurately predicting OH chemistry and ozone production.

651 In the FT, the model exhibits a persistent low bias (~60%) for VOC-carbon and reactivity that manifests  
652 essentially everywhere. A comparison of modeled versus observed PBL:FT VOC concentration ratios  
653 over the southeastern US suggests that inadequate PBL ventilation in the model may play a role in driving  
654 the observed FT biases. Recent work has sought to improve CTM transport performance through  
655 improved spatial resolution (e.g., (Zhuang et al., 2018; Yu et al., 2016)), through use of a cubed-sphere  
656 rather than regular Cartesian grid (e.g., (Eastham et al., 2018; Yu et al., 2018)), and by integration into



657 earth system models with online coupled meteorology (e.g., (Hu et al., 2018; Long et al., 2015)). Further  
658 work is needed to specifically assess model treatment of PBL-FT coupling (e.g., using PAN:NO<sub>x</sub> or other  
659 diagnostic quantities) and PBL depths to improve tracer simulations in the FT.

660 We used a source tracer analysis to investigate the likely role of biogenic versus anthropogenic sources in  
661 driving model biases for key oxygenated VOCs. Results point to a current overestimate of the (primary +  
662 secondary) biogenic sources of hydroxyacetone, methyl ethyl ketone, and glyoxal and an underestimate of  
663 the biogenic sources of formic acid. Results also suggest a possible underestimate of the anthropogenic  
664 sources of acetaldehyde, along with an underestimate of peroxyacetic acid production across both  
665 biogenic and anthropogenic precursors. Finally, we find that a relatively modest number of individual  
666 VOCs (acetone, methanol, ethane, acetaldehyde, formaldehyde, isoprene + oxidation products, methyl  
667 hydroperoxide) drive a significant fraction of the total ambient VOC-carbon and reactivity (and  
668 associated model biases) across many environments. These species therefore merit further research to  
669 better understand their budgets and to improve model representation of VOC chemistry and the resulting  
670 effects on SOA, O<sub>3</sub>, and other oxidants.

671

#### 672 **Data availability**

673 Aircraft data used here are available at NASA LaRC (<https://www-air.larc.nasa.gov/missions.htm>) and  
674 NOAA ESRL ESD (<https://esrl.noaa.gov/csd/field.html>). GEOS-Chem model code is available at  
675 [www.geos-chem.org](http://www.geos-chem.org).

676

#### 677 **Author contributions**

678 X. Chen, D. B. Millet, H. B. Singh, and A. Wisthaler designed the study. X. Chen and D. B. Millet led the  
679 model development, simulations, all analyses, and manuscript preparation. The following authors  
680 provided measurements used in the analysis and contributed to manuscript preparation and data  
681 interpretation: A. Wisthaler, T. Mikoviny, and M. Müller (DC3, SEAC<sup>4</sup>RS, and DISCOVER-AQ PTR-  
682 MS), E. C. Apel and H. S. Hornbrook (TOGA), E. L. Atlas (CalNex WAS), D. R. Blake (CalNex,  
683 SEAC<sup>4</sup>RS, and FRAPPÉ WAS), S. S. Brown, K.-E. Min, and R. A. Washenfelder (SENEX glyoxal), J.  
684 D. Crouse (CIT-CIMS), J. A. de Gouw and C. Warneke (CalNex and SENEX PTR-MS), F. Flocke, G.  
685 G. Pfister, and S. Shertz (FRAPPÉ PTR-MS and PAN-CIMS), A. Fried, D. Richter, J. Walega, and P.  
686 Weibring (DFGAS and CAMS formaldehyde), B. G. Heikes, D. W. O'Sullivan, and V. Treadaway  
687 (PCIMS), J. A. Neuman (SENEX NOAA CIMS HCOOH), T. B. Ryerson and J. Peischl (NOAA NO<sub>y</sub>O<sub>3</sub>),  
688 J. M. Roberts (CalNex and SENEX PAN), P. R. Veres (SENEX PAN), and B. Yuan (other PTR-MS  
689 data).

690

#### 691 **Acknowledgements**

692 This research was supported by NASA Atmospheric Composition Campaign Data Analysis and  
693 Modelling (ACCDAM) program (Grant NNX14AP89G). Computing resources were provided by the  
694 Minnesota Supercomputing Institute (<https://www.msi.umn.edu>) at the University of Minnesota. We  
695 acknowledge the ECCAD database (<http://eccad.sedoo.fr>) for hosting emission inventories used in this  
696 work. We thank Kelley Wells, Katie Travis, Seb Eastham, Joel Thornton, Paul Wennberg, Gao Chen for  
697 their assistance and useful discussions.

698 We thank the CalNex, DC3, SENEX, SEAC<sup>4</sup>RS, DISCOVER-AQ, and FRAPPÉ teams for making this  
699 work possible. In particular, we acknowledge the contributions of Martin Graus (SENEX PTR-MS),





700 Jessica Gilman (SENEX WAS), Lisa Kaser (FRAPPÉ PTR-MS), Joel Thornton, Ben Lee and Felipe  
701 Lopez-Hilfiker (UW CIMS), Thomas Hanisco and Glenn Wolfe (ISAF-LIF), Ronald Cohen (TD-LIF),  
702 Greg Huey (GIT CIMS), Andrew Weinheimer (NCAR NO<sub>x</sub>/NO<sub>y</sub>), and Tara Yacovitch and Scott Herndon  
703 (DISCOVER-AQ Colorado ethane).

704 A.W. acknowledges the Austrian Federal Ministry for Transport, Innovation and Technology (bmvit)  
705 through the Austrian Space Applications Programme (ASAP) of the Austrian Research Promotion  
706 Agency (FFG) for supporting the PTR-MS measurements during DC3, SEAC<sup>4</sup>RS and DISCOVER-AQ.  
707 T.M. was supported by an appointment to the NASA Postdoctoral Program at the Langley Research  
708 Center administered by Oak Ridge Associated Universities through a contract with NASA.

709 F.F. and G.P. thank the State of Colorado/Colorado Department of Public Health and Environment and  
710 the National Science Foundation (NSF) for funding of FRAPPÉ. The National Center for Atmospheric  
711 Research is sponsored by NSF.

712

713 **References**

- 714 Akagi, S. K., Yokelson, R. J., Wiedinmyer, C., Alvarado, M. J., Reid, J. S., Karl, T., Crouse, J. D., and Wennberg, P. O.:  
715 Emission factors for open and domestic biomass burning for use in atmospheric models, *Atmos. Chem. Phys.*, 11, 4039-4072,  
716 <https://doi.org/10.5194/acp-11-4039-2011>, 2011.
- 717 Amos, H. M., Jacob, D. J., Holmes, C. D., Fisher, J. A., Wang, Q., Yantosca, R. M., Corbitt, E. S., Galarneau, E., Rutter, A. P.,  
718 Gustin, M. S., Steffen, A., Schauer, J. J., Graydon, J. A., St Louis, V. L., Talbot, R. W., Edgerton, E. S., Zhang, Y., and  
719 Sunderland, E. M.: Gas-particle partitioning of atmospheric Hg(II) and its effect on global mercury deposition, *Atmos. Chem.*  
720 *Phys.*, 12, 591-603, <https://doi.org/10.5194/acp-12-591-2012>, 2012.
- 721 Andreae, M. O., and Merlet, P.: Emission of trace gases and aerosols from biomass burning, *Global Biogeochem Cy*, 15, 955-  
722 966, <https://doi.org/10.1029/2000gb001382>, 2001.
- 723 Apel, E. C., Emmons, L. K., Karl, T., Flocke, F., Hills, A. J., Madronich, S., Lee-Taylor, J., Fried, A., Weibring, P., Walega, J.,  
724 Richter, D., Tie, X., Mauldin, L., Campos, T., Weinheimer, A., Knapp, D., Sive, B., Kleinman, L., Springston, S., Zaveri, R.,  
725 Ortega, J., Voss, P., Blake, D., Baker, A., Warneke, C., Welsh-Bon, D., de Gouw, J., Zheng, J., Zhang, R., Rudolph, J.,  
726 Junkermann, W., and Riemer, D. D.: Chemical evolution of volatile organic compounds in the outflow of the Mexico City  
727 Metropolitan area, *Atmos. Chem. Phys.*, 10, 2353-2375, <https://doi.org/10.5194/acp-10-2353-2010>, 2010.
- 728 Apel, E. C., Hornbrook, R. S., Hills, A. J., Blake, N. J., Barth, M. C., Weinheimer, A., Cantrell, C., Rutledge, S. A., Basarab, B.,  
729 Crawford, J., Diskin, G., Homeyer, C. R., Campos, T., Flocke, F., Fried, A., Blake, D. R., Brune, W., Pollack, I., Peischl, J.,  
730 Ryerson, T., Wennberg, P. O., Crouse, J. D., Wisthaler, A., Mikoviny, T., Huey, G., Heikes, B., O'Sullivan, D., and Riemer, D.  
731 D.: Upper tropospheric ozone production from lightning NO<sub>x</sub>-impacted convection: Smoke ingestion case study from the DC3  
732 campaign, *J. Geophys. Res. Atmos.*, 120, 2505-2523, <https://doi.org/10.1002/2014JD022121>, 2015.
- 733 Barth, M. C., Cantrell, C. A., Brune, W. H., Rutledge, S. A., Crawford, J. H., Huntrieser, H., Carey, L. D., MacGorman, D.,  
734 Weisman, M., Pickering, K. E., Bruning, E., Anderson, B., Apel, E., Biggerstaff, M., Campos, T., Campuzano-Jost, P., Cohen,  
735 R., Crouse, J., Day, D. A., Diskin, G., Flocke, F., Fried, A., Garland, C., Heikes, B., Honomichl, S., Hornbrook, R., Huey, L. G.,  
736 Jimenez, J. L., Lang, T., Lichtenstern, M., Mikoviny, T., Nault, B., O'Sullivan, D., Pan, L. L., Peischl, J., Pollack, I., Richter, D.,  
737 Riemer, D., Ryerson, T., Schlager, H., St Clair, J., Walega, J., Weibring, P., Weinheimer, A., Wennberg, P., Wisthaler, A.,  
738 Wooldridge, P. J., and Ziegler, C.: The Deep Convective Clouds and Chemistry (DC3) Field Campaign, *B Am Meteorol Soc*, 96,  
739 1281-1309, <https://doi.org/10.1175/Bams-D-13-00290.1>, 2015.
- 740 Beale, R., Liss, P. S., Dixon, J. L., and Nightingale, P. D.: Quantification of oxygenated volatile organic compounds in seawater  
741 by membrane inlet-proton transfer reaction/mass spectrometry, *Anal. Chim. Acta*, 706, 128-134,  
742 <https://doi.org/10.1016/j.aca.2011.08.023>, 2011.
- 743 Beale, R., Dixon, J. L., Arnold, S. R., Liss, P. S., and Nightingale, P. D.: Methanol, acetaldehyde, and acetone in the surface  
744 waters of the Atlantic Ocean, *J. Geophys. Res. Oceans*, 118, 5412-5425, <https://doi.org/10.1002/jgrc.20322>, 2013.
- 745 Beale, R., Dixon, J. L., Smyth, T. J., and Nightingale, P. D.: Annual study of oxygenated volatile organic compounds in UK shelf  
746 waters, *Mar. Chem.*, 171, 96-106, <https://doi.org/10.1016/j.marchem.2015.02.013>, 2015.
- 747 Bertram, T. H., Perring, A. E., Wooldridge, P. J., Crouse, J. D., Kwan, A. J., Wennberg, P. O., Scheuer, E., Dibb, J., Avery, M.,  
748 Sachse, G., Vay, S. A., Crawford, J. H., McNaughton, C. S., Clarke, A., Pickering, K. E., Fuelberg, H., Huey, G., Blake, D. R.,  
749 Singh, H. B., Hall, S. R., Shetter, R. E., Fried, A., Heikes, B. G., and Cohen, R. C.: Direct measurements of the convective  
750 recycling of the upper troposphere, *Science*, 315, 816-820, <https://doi.org/10.1126/science.1134548>, 2007.
- 751 Bianchi, F., Trostl, J., Junninen, H., Frege, C., Henne, S., Hoyle, C. R., Molteni, U., Herrmann, E., Adamov, A., Bukowiecki, N.,  
752 Chen, X., Duplissy, J., Gysel, M., Hutterli, M., Kangasluoma, J., Kontkanen, J., Kurten, A., Manninen, H. E., Munch, S.,  
753 Perakyla, O., Petaja, T., Rondo, L., Williamson, C., Weingartner, E., Curtius, J., Worsnop, D. R., Kulmala, M., Dommen, J., and  
754 Baltensperger, U.: New particle formation in the free troposphere: A question of chemistry and timing, *Science*, 352, 1109-1112,  
755 <https://doi.org/10.1126/science.aad5456>, 2016.
- 756 Blake, N. J., Blake, D. R., Swanson, A. L., Atlas, E., Flocke, F., and Rowland, F. S.: Latitudinal, vertical, and seasonal variations  
757 of C<sub>1</sub>-C<sub>4</sub> alkyl nitrates in the troposphere over the Pacific Ocean during PEM-Tropics A and B: Oceanic and continental sources,  
758 *J. Geophys. Res. Atmos.*, 108, <https://doi.org/10.1029/2001jd001444>, 2003.
- 759 Bonsang, B., Kanakidou, M., Lambert, G., and Monfray, P.: The marine source of C<sub>2</sub>-C<sub>6</sub> aliphatic-hydrocarbons, *J. Atmos.*  
760 *Chem.*, 6, 3-20, <https://doi.org/10.1007/Bf00048328>, 1988.



- 761 Boucher, O., Randall, D., Artaxo, P., Bretherton, C., Feingold, G., Forster, C., Kerminen, V. M., Kondo, Y., Liao, H., Lohmann,  
762 U., Rasch, P., Sathesh, S. K., Sherwood, S., and Stevens, B.: Clouds and aerosols, in: *Climate Change 2013: The Physical  
763 Science Basis. Contribution of Working Group I to the Fifth Assessment Report of the Intergovernmental Panel on Climate  
764 Change*, edited by: Stocker, T. F., Qin, D., Plattner, G.-K., Tignor, M., Allen, S. K., Boschung, J., Nauels, A., Xia, Y., Bex, V.,  
765 and Midgley, P. M., Cambridge University Press, Cambridge, United Kingdom and New York, NY, USA, 571–658, 2013.
- 766 Broadgate, W. J., Liss, P. S., and Penkett, S. A.: Seasonal emissions of isoprene and other reactive hydrocarbon gases from the  
767 ocean, *Geophys Res Lett*, 24, 2675-2678, <https://doi.org/10.1029/97gl02736>, 1997.
- 768 Brune, W. H., Ren, X. R., Zhang, L., Mao, J. Q., Miller, D. O., Anderson, B. E., Blake, D. R., Cohen, R. C., Diskin, G. S., Hall,  
769 S. R., Hanisco, T. F., Huey, L. G., Nault, B. A., Peisch, J., Pollack, I., Ryerson, T. B., Shingler, T., Sorooshian, A., Ullmann, K.,  
770 Wisthaler, A., and Wooldridge, P. J.: Atmospheric oxidation in the presence of clouds during the Deep Convective Clouds and  
771 Chemistry (DC3) study, *Atmos. Chem. Phys.*, 18, 14493-14510, <https://doi.org/10.5194/acp-18-14493-2018>, 2018.
- 772 Cappa, C.: Atmospheric science: Unexpected player in particle formation, *Nature*, 533, 478-479,  
773 <https://doi.org/10.1038/533478a>, 2016.
- 774 Caravan, R. L., Khan, M. A. H., Zador, J., Sheps, L., Antonov, I. O., Rotavera, B., Ramasesha, K., Au, K., Chen, M. W., Rosch,  
775 D., Osborn, D. L., Fittschen, C., Schoemaeker, C., Duncianu, M., Grira, A., Dusanter, S., Tomas, A., Percival, C. J., Shallcross,  
776 D. E., and Taatjes, C. A.: The reaction of hydroxyl and methylperoxy radicals is not a major source of atmospheric methanol,  
777 *Nat. Commun.*, 9, 4343, <https://doi.org/10.1038/s41467-018-06716-x>, 2018.
- 778 Carpenter, L. J., Archer, S. D., and Beale, R.: Ocean-atmosphere trace gas exchange, *Chem. Soc. Rev.*, 41, 6473-6506,  
779 <https://doi.org/10.1039/c2cs35121h>, 2012.
- 780 Cazorla, M., Wolfé, G. M., Bailey, S. A., Swanson, A. K., Arkinson, H. L., and Hanisco, T. F.: A new airborne laser-induced  
781 fluorescence instrument for in situ detection of formaldehyde throughout the troposphere and lower stratosphere, *Atmos. Meas.  
782 Tech.*, 8, 541-552, <https://doi.org/10.5194/amt-8-541-2015>, 2015.
- 783 Coburn, S., Ortega, I., Thalman, R., Blomquist, B., Fairall, C. W., and Volkamer, R.: Measurements of diurnal variations and  
784 eddy covariance (EC) fluxes of glyoxal in the tropical marine boundary layer: description of the Fast LED-CE-DOAS instrument,  
785 *Atmos. Meas. Tech.*, 7, 3579-3595, <https://doi.org/10.5194/amt-7-3579-2014>, 2014.
- 786 Colman, J. J., Swanson, A. L., Meinardi, S., Sive, B. C., Blake, D. R., and Rowland, F. S.: Description of the analysis of a wide  
787 range of volatile organic compounds in whole air samples collected during PEM-tropics A and B, *Anal. Chem.*, 73, 3723-3731,  
788 <https://doi.org/10.1021/ac010027g>, 2001.
- 789 Crawford, J. H., and Pickering, K. E.: Advancing Strategies for Air Quality Observations in the Next Decade, *Environ. Manage.*,  
790 4-7, 2014.
- 791 Crouse, J. D., McKinney, K. A., Kwan, A. J., and Wennberg, P. O.: Measurement of gas-phase hydroperoxides by chemical  
792 ionization mass spectrometry, *Anal. Chem.*, 78, 6726-6732, <https://doi.org/10.1021/ac0604235>, 2006.
- 793 Crouse, J. D., Nielsen, L. B., Jørgensen, S., Kjaergaard, H. G., and Wennberg, P. O.: Autoxidation of Organic Compounds in  
794 the Atmosphere, *J. Phys. Chem. Lett.*, 4, 3513-3520, <https://doi.org/10.1021/jz4019207>, 2013.
- 795 Cubasch, U., Wuebbles, D., Chen, D., Facchini, M. C., Frame, C. L., Mahowald, N., and Winther, J.-G.: Introduction, in: *Climate  
796 Change 2013: The Physical Science Basis. Contribution of Working Group I to the Fifth Assessment Report of the  
797 Intergovernmental Panel on Climate Change*, edited by: Stocker, T. F., Qin, D., Plattner, G.-K., Tignor, M., Allen, S. K.,  
798 Boschung, J., Nauels, A., Xia, Y., Bex, V., and Midgley, P. M., Cambridge University Press, Cambridge, United Kingdom and  
799 New York, NY, USA, 119–158, 2013.
- 800 Curry, L. A., Tsui, W. G., and McNeill, V. F.: Technical note: Updated parameterization of the reactive uptake of glyoxal and  
801 methylglyoxal by atmospheric aerosols and cloud droplets, *Atmos. Chem. Phys.*, 18, 9823-9830, <https://doi.org/10.5194/acp-18-9823-2018>, 2018.
- 803 DC3 Science Team: DC3 Field Campaign Data from DC-8 aircraft. NASA Langley Atmospheric Science Data Center DAAC,  
804 <https://doi.org/10.5067/aircraft/dc3/dc8/aerosol-tracegas>, 2013.



- 805 de Gouw, J., and Warneke, C.: Measurements of volatile organic compounds in the earth's atmosphere using proton-transfer-  
806 reaction mass spectrometry, *Mass Spectrom. Rev.*, 26, 223-257, <https://doi.org/10.1002/mas.20119>, 2007.
- 807 de Gouw, J. A., Middlebrook, A. M., Warneke, C., Goldan, P. D., Kuster, W. C., Roberts, J. M., Fehsenfeld, F. C., Worsnop, D.  
808 R., Canagaratna, M. R., Pszenny, A. A. P., Keene, W. C., Marchewka, M., Bertman, S. B., and Bates, T. S.: Budget of organic  
809 carbon in a polluted atmosphere: Results from the New England Air Quality Study in 2002, *J. Geophys. Res. Atmos.*, 110,  
810 <https://doi.org/10.1029/2004jd005623>, 2005.
- 811 de Gouw, J. A., Gilman, J. B., Borbon, A., Warneke, C., Kuster, W. C., Goldan, P. D., Holloway, J. S., Peischl, J., Ryerson, T.  
812 B., Parrish, D. D., Gentner, D. R., Goldstein, A. H., and Harley, R. A.: Increasing atmospheric burden of ethanol in the United  
813 States, *Geophys Res Lett*, 39, <https://doi.org/10.1029/2012gl052109>, 2012.
- 814 Deventer, M. J., Jiao, Y., Knox, H., Anderson, F., Ferner, M. C., Lewis, J. A., and Rhew, R. C.: Ecosystem-scale measurements  
815 of methyl halide fluxes from a brackish tidal marsh invaded with perennial pepperweed (*lepidium latifolium*), *J. Geophys. Res.*  
816 *Biogeosci.*, 123, 2104-2120, <https://doi.org/10.1029/2018JG004536>, 2018.
- 817 DiGangi, J. P., Boyle, E. S., Karl, T., Harley, P., Turnipseed, A., Kim, S., Cantrell, C., Maudlin, R. L., Zheng, W., Flocke, F.,  
818 Hall, S. R., Ullmann, K., Nakashima, Y., Paul, J. B., Wolfe, G. M., Desai, A. R., Kajii, Y., Guenther, A., and Keutsch, F. N.:  
819 First direct measurements of formaldehyde flux via eddy covariance: implications for missing in-canopy formaldehyde sources,  
820 *Atmos. Chem. Phys.*, 11, 10565-10578, <https://doi.org/10.5194/acp-11-10565-2011>, 2011.
- 821 DISCOVER-AQ Science Team: DISCOVER-AQ P-3B Aircraft In-situ Trace Gas Measurements. NASA Langley Atmospheric  
822 Science Data Center DAAC, <https://doi.org/10.5067/aircraft/discover-aq/aerosol-tracegas>, 2014.
- 823 Eastham, S. D., Long, M. S., Keller, C. A., Lundgren, E., Yantosca, R. M., Zhuang, J., Li, C., Lee, C. J., Yannetti, M., and Auer,  
824 B. M.: GEOS-Chem High Performance (GCHP v11-02c): a next-generation implementation of the GEOS-Chem chemical  
825 transport model for massively parallel applications, *Geosci Model Dev*, 11, 2941-2953, 2018.
- 826 Ehn, M., Thornton, J. A., Kleist, E., Sipila, M., Junninen, H., Pullinen, I., Springer, M., Rubach, F., Tillmann, R., Lee, B., Lopez-  
827 Hilfiker, F., Andres, S., Acir, I. H., Rissanen, M., Jokinen, T., Schobesberger, S., Kangasluoma, J., Kontkanen, J., Nieminen, T.,  
828 Kurten, T., Nielsen, L. B., Jorgensen, S., Kjaergaard, H. G., Canagaratna, M., Maso, M. D., Berndt, T., Petaja, T., Wahner, A.,  
829 Kerminen, V. M., Kulmala, M., Worsnop, D. R., Wildt, J., and Mentel, T. F.: A large source of low-volatility secondary organic  
830 aerosol, *Nature*, 506, 476-479, <https://doi.org/10.1038/nature13032>, 2014.
- 831 EPA: 2011 National Emissions Inventory Data & Documentation, available at: [https://www.epa.gov/air-emissions-](https://www.epa.gov/air-emissions-inventories/2011-national-emission-inventory-nei-report)  
832 [inventories/2011-national-emission-inventory-nei-report](https://www.epa.gov/air-emissions-inventories/2011-national-emission-inventory-nei-report), last access: 8 Feb 2018, 2015.
- 833 EPA: Technical Support Document EPA's 2014 National Air Toxics Assessment, available at:  
834 [https://www.epa.gov/sites/production/files/2018-09/documents/2014\\_nata\\_technical\\_support\\_document.pdf](https://www.epa.gov/sites/production/files/2018-09/documents/2014_nata_technical_support_document.pdf) last access: 25 Sep  
835 2018, 2018.
- 836 European Commission (EC): Joint Research Centre (JRC)/Netherlands Environmental Assessment Agency (PBL), Emission  
837 Database for Global Atmospheric Research (EDGAR), release version 4.2. <http://edgar.jrc.ec.europa.eu>, 2011.
- 838 Feiner, P. A., Brune, W. H., Miller, D. O., Zhang, L., Cohen, R. C., Romer, P. S., Goldstein, A. H., Keutsch, F. N., Skog, K. M.,  
839 Wennberg, P. O., Nguyen, T. B., Teng, A. P., DeGouw, J., Koss, A., Wild, R. J., Brown, S. S., Guenther, A., Edgerton, E.,  
840 Baumann, K., and Fry, J. L.: Testing atmospheric oxidation in an Alabama forest, *J Atmos Sci*, 73, 4699-4710,  
841 <https://doi.org/10.1175/Jas-D-16-0044.1>, 2016.
- 842 Fischer, E. V., Jacob, D. J., Millet, D. B., Yantosca, R. M., and Mao, J.: The role of the ocean in the global atmospheric budget of  
843 acetone, *Geophys Res Lett*, 39, n/a-n/a, <https://doi.org/10.1029/2011gl050086>, 2012.
- 844 Fischer, E. V., Jacob, D. J., Yantosca, R. M., Sulprizio, M. P., Millet, D. B., Mao, J., Paulot, F., Singh, H. B., Roiger, A., Ries,  
845 L., Talbot, R. W., Dzepina, K., and Deolal, S. P.: Atmospheric peroxyacetyl nitrate (PAN): a global budget and source  
846 attribution, *Atmos. Chem. Phys.*, 14, 2679-2698, <https://doi.org/10.5194/acp-14-2679-2014>, 2014.
- 847 Fisher, J. A., Jacob, D. J., Travis, K. R., Kim, P. S., Marais, E. A., Miller, C. C., Yu, K., Zhu, L., Yantosca, R. M., Sulprizio, M.  
848 P., Mao, J., Wennberg, P. O., Crouse, J. D., Teng, A. P., Nguyen, T. B., St Clair, J. M., Cohen, R. C., Romer, P., Nault, B. A.,  
849 Wooldridge, P. J., Jimenez, J. L., Campuzano-Jost, P., Day, D. A., Hu, W., Shepson, P. B., Xiong, F., Blake, D. R., Goldstein, A.  
850 H., Misztal, P. K., Hanisco, T. F., Wolfe, G. M., Ryerson, T. B., Wisthaler, A., and Mikoviny, T.: Organic nitrate chemistry and



- 851 its implications for nitrogen budgets in an isoprene- and monoterpene-rich atmosphere: constraints from aircraft (SEAC(4)RS)  
852 and ground-based (SOAS) observations in the Southeast US, *Atmos. Chem. Phys.*, 16, 5969-5991, <https://doi.org/10.5194/acp->  
853 16-5969-2016, 2016.
- 854 Fried, A., Cantrell, C., Olson, J., Crawford, J. H., Weibring, P., Walega, J., Richter, D., Junkermann, W., Volkamer, R., Sinreich,  
855 R., Heikes, B. G., O'Sullivan, D., Blake, D. R., Blake, N., Meinardi, S., Apel, E., Weinheimer, A., Knapp, D., Perring, A., Cohen,  
856 R. C., Fuelberg, H., Shetter, R. E., Hall, S. R., Ullmann, K., Brune, W. H., Mao, J., Ren, X., Huey, L. G., Singh, H. B., Hair, J.  
857 W., Riemer, D., Diskin, G., and Sachse, G.: Detailed comparisons of airborne formaldehyde measurements with box models  
858 during the 2006 INTEX-B and MILAGRO campaigns: potential evidence for significant impacts of unmeasured and multi-  
859 generation volatile organic carbon compounds, *Atmos. Chem. Phys.*, 11, 11867-11894, <https://doi.org/10.5194/acp-11-11867->  
860 2011, 2011.
- 861 Giglio, L., Randerson, J. T., and van der Werf, G. R.: Analysis of daily, monthly, and annual burned area using the fourth-  
862 generation global fire emissions database (GFED4), *J. Geophys. Res. Biogeosci.*, 118, 317-328,  
863 <https://doi.org/10.1002/jgrg.20042>, 2013.
- 864 Gilman, J. B., Kuster, W. C., Goldan, P. D., Herndon, S. C., Zahniser, M. S., Tucker, S. C., Brewer, W. A., Lerner, B. M.,  
865 Williams, E. J., Harley, R. A., Fehsenfeld, F. C., Warneke, C., and de Gouw, J. A.: Measurements of volatile organic compounds  
866 during the 2006 TexAQs/GoMACCS campaign: Industrial influences, regional characteristics, and diurnal dependencies of the  
867 OH reactivity, *J. Geophys. Res. Atmos.*, 114, <https://doi.org/10.1029/2008jd011525>, 2009.
- 868 Glasius, M., and Goldstein, A. H.: Recent discoveries and future challenges in atmospheric organic chemistry, *Environ. Sci.*  
869 *Technol.*, 50, 2754-2764, <https://doi.org/10.1021/acs.est.5b05105>, 2016.
- 870 Goldstein, A. H., and Galbally, I. E.: Known and unexplored organic constituents in the earth's atmosphere, *Environ. Sci.*  
871 *Technol.*, 41, 1514-1521, <https://doi.org/10.1021/Es072476p>, 2007.
- 872 Guenther, A. B., Jiang, X., Heald, C. L., Sakulyanontvittaya, T., Duhl, T., Emmons, L. K., and Wang, X.: The Model of  
873 Emissions of Gases and Aerosols from Nature version 2.1 (MEGAN2.1): an extended and updated framework for modeling  
874 biogenic emissions, *Geosci Model Dev*, 5, 1471-1492, <https://doi.org/10.5194/gmd-5-1471-2012>, 2012.
- 875 Hatch, L. E., Yokelson, R. J., Stockwell, C. E., Veres, P. R., Simpson, I. J., Blake, D. R., Orlando, J. J., and Barsanti, K. C.:  
876 Multi-instrument comparison and compilation of non-methane organic gas emissions from biomass burning and implications for  
877 smoke-derived secondary organic aerosol precursors, *Atmos. Chem. Phys.*, 17, 1471-1489, <https://doi.org/10.5194/acp-17-1471->  
878 2017, 2017.
- 879 Heald, C. L., Jacob, D. J., Park, R. J., Russell, L. M., Huebert, B. J., Seinfeld, J. H., Liao, H., and Weber, R. J.: A large organic  
880 aerosol source in the free troposphere missing from current models, *Geophys Res Lett*, 32, n/a-n/a,  
881 <https://doi.org/10.1029/2005gl023831>, 2005.
- 882 Heald, C. L., Goldstein, A. H., Allan, J. D., Aiken, A. C., Apel, E., Atlas, E. L., Baker, A. K., Bates, T. S., Beyersdorf, A. J.,  
883 Blake, D. R., Campos, T., Coe, H., Crouse, J. D., DeCarlo, P. F., de Gouw, J. A., Dunlea, E. J., Flocke, F. M., Fried, A., Goldan,  
884 P., Griffin, R. J., Herndon, S. C., Holloway, J. S., Holzinger, R., Jimenez, J. L., Junkermann, W., Kuster, W. C., Lewis, A. C.,  
885 Meinardi, S., Millet, D. B., Onasch, T., Polidori, A., Quinn, P. K., Riemer, D. D., Roberts, J. M., Salcedo, D., Sive, B., Swanson,  
886 A. L., Talbot, R., Warneke, C., Weber, R. J., Weibring, P., Wennberg, P. O., Worsnop, D. R., Wittig, A. E., Zhang, R., Zheng, J.,  
887 and Zheng, W.: Total observed organic carbon (TOOC) in the atmosphere: a synthesis of North American observations, *Atmos.*  
888 *Chem. Phys.*, 8, 2007-2025, <https://doi.org/10.5194/acp-8-2007-2008>, 2008.
- 889 Hottle, J. R., Huisman, A. J., DiGangi, J. P., Kammrath, A., Galloway, M. M., Coens, K. L., and Keutsch, F. N.: A laser induced  
890 fluorescence-based instrument for in-situ measurements of atmospheric formaldehyde, *Environ. Sci. Technol.*, 43, 790-795,  
891 <https://doi.org/10.1021/es801621f>, 2009.
- 892 Hu, L., Millet, D. B., Baasandorj, M., Griffis, T. J., Turner, P., Helmig, D., Curtis, A. J., and Hueber, J.: Isoprene emissions and  
893 impacts over an ecological transition region in the US Upper Midwest inferred from tall tower measurements, *J. Geophys. Res.*  
894 *Atmos.*, 120, 3553-3571, <https://doi.org/10.1002/2014JD022732>, 2015.
- 895 Hu, L., Keller, C. A., Long, M. S., Sherwen, T., Auer, B., Da Silva, A., Nielsen, J. E., Pawson, S., Thompson, M. A., Trayanov,  
896 A. L., Travis, K. R., Grange, S. K., Evans, M. J., and Jacob, D. J.: Global simulation of tropospheric chemistry at 12.5 km  
897 resolution: performance and evaluation of the GEOS-Chem chemical module (v10-1) within the NASA GEOS Earth system  
898 model (GEOS-5 ESM), *Geosci Model Dev*, 11, 4603-4620, <https://doi.org/10.5194/gmd-11-4603-2018>, 2018.



- 899 Hudman, R. C., Moore, N. E., Mebust, A. K., Martin, R. V., Russell, A. R., Valin, L. C., and Cohen, R. C.: Steps towards a  
900 mechanistic model of global soil nitric oxide emissions: implementation and space based-constraints, *Atmos. Chem. Phys.*, 12,  
901 7779-7795, <https://doi.org/10.5194/acp-12-7779-2012>, 2012.
- 902 Hudson, E. D., Okuda, K., and Ariya, P. A.: Determination of acetone in seawater using derivatization solid-phase  
903 microextraction, *Anal. Bioanal. Chem.*, 388, 1275-1282, <https://doi.org/10.1007/s00216-007-1324-x>, 2007.
- 904 Huey, L. G.: Measurement of trace atmospheric species by chemical ionization mass spectrometry: speciation of reactive  
905 nitrogen and future directions, *Mass Spectrom. Rev.*, 26, 166-184, <https://doi.org/10.1002/mas.20118>, 2007.
- 906 Hunter, J. F., Day, D. A., Palm, B. B., Yatavelli, R. L. N., Chan, A. H., Kaser, L., Cappellin, L., Hayes, P. L., Cross, E. S.,  
907 Carrasquillo, A. J., Campuzano-Jost, P., Stark, H., Zhao, Y. L., Hohaus, T., Smith, J. N., Hansel, A., Karl, T., Goldstein, A. H.,  
908 Guenther, A., Worsnop, D. R., Thornton, J. A., Heald, C. L., Jimenez, J. L., and Kroll, J. H.: Comprehensive characterization of  
909 atmospheric organic carbon at a forested site, *Nat Geosci*, 10, 748+, <https://doi.org/10.1038/NGEO3018>, 2017.
- 910 Iavorivska, L., Boyer, E. W., and Grimm, J. W.: Wet atmospheric deposition of organic carbon: An underreported source of  
911 carbon to watersheds in the northeastern United States, *J. Geophys. Res. Atmos.*, 122, 3104-3115,  
912 <https://doi.org/10.1002/2016JD026027>, 2017.
- 913 Isaacman-VanWertz, G., Massoli, P., O'Brien, R., Lim, C., Franklin, J. P., Moss, J. A., Hunter, J. F., Nowak, J. B., Canagaratna,  
914 M. R., Misztal, P. K., Arata, C., Roscioli, J. R., Herndon, S. T., Onasch, T. B., Lambe, A. T., Jayne, J. T., Su, L., Knopf, D. A.,  
915 Goldstein, A. H., Worsnop, D. R., and Kroll, J. H.: Chemical evolution of atmospheric organic carbon over multiple generations  
916 of oxidation, *Nat. Chem.*, 10, 462-468, <https://doi.org/10.1038/s41557-018-0002-2>, 2018.
- 917 Jacob, D. J.: Heterogeneous chemistry and tropospheric ozone, *Atmos. Environ.*, 34, 2131-2159, [https://doi.org/10.1016/S1352-2310\(99\)00462-8](https://doi.org/10.1016/S1352-2310(99)00462-8), 2000.
- 919 Johnson, M. T.: A numerical scheme to calculate temperature and salinity dependent air-water transfer velocities for any gas,  
920 *Ocean Sci.*, 6, 913-932, <https://doi.org/10.5194/os-6-913-2010>, 2010.
- 921 Kaiser, J., Skog, K. M., Baumann, K., Bertman, S. B., Brown, S. B., Brune, W. H., Crounse, J. D., de Gouw, J. A., Edgerton, E.  
922 S., Feiner, P. A., Goldstein, A. H., Koss, A., Misztal, P. K., Nguyen, T. B., Olson, K. F., St Clair, J. M., Teng, A. P., Toma, S.,  
923 Wennberg, P. O., Wild, R. J., Zhang, L., and Keutsch, F. N.: Speciation of OH reactivity above the canopy of an isoprene-  
924 dominated forest, *Atmos. Chem. Phys.*, 16, 9349-9359, <https://doi.org/10.5194/acp-16-9349-2016>, 2016.
- 925 Kaiser, J., Jacob, D. J., Zhu, L., Travis, K. R., Fisher, J. A., Abad, G. G., Zhang, L., Zhang, X. S., Fried, A., Crounse, J. D., St  
926 Clair, J. M., and Wisthaler, A.: High-resolution inversion of OMI formaldehyde columns to quantify isoprene emission on  
927 ecosystem-relevant scales: application to the southeast US, *Atmos. Chem. Phys.*, 18, 5483-5497, <https://doi.org/10.5194/acp-18-5483-2018>, 2018.
- 929 Kameyama, S., Tanimoto, H., Inomata, S., Tsunogai, U., Ooki, A., Yokouchi, Y., Takeda, S., Obata, H., and Uematsu, M.:  
930 Equilibrator inlet-proton transfer reaction-mass spectrometry (EI-PTR-MS) for sensitive, high-resolution measurement of  
931 dimethyl sulfide dissolved in seawater, *Anal. Chem.*, 81, 9021-9026, <https://doi.org/10.1021/ac901630h>, 2009.
- 932 Kanakidou, M., Bonsang, B., Lerouille, J. C., Lambert, G., Martin, D., and Sennequier, G.: Marine source of atmospheric  
933 acetylene, *Nature*, 333, 51-52, <https://doi.org/10.1038/333051a0>, 1988.
- 934 Kanakidou, M., Duce, R. A., Prospero, J. M., Baker, A. R., Benitez-Nelson, C., Dentener, F. J., Hunter, K. A., Liss, P. S.,  
935 Mahowald, N., Okin, G. S., Sarin, M., Tsigaridis, K., Uematsu, M., Zamora, L. M., and Zhu, T.: Atmospheric fluxes of organic N  
936 and P to the global ocean, *Global Biogeochem Cy*, 26, <https://doi.org/10.1029/2011gb004277>, 2012.
- 937 Karl, T., Harley, P., Emmons, L., Thornton, B., Guenther, A., Basu, C., Turnipseed, A., and Jardine, K.: Efficient atmospheric  
938 cleansing of oxidized organic trace gases by vegetation, *Science*, 330, 816-819, <https://doi.org/10.1126/science.1192534>, 2010.
- 939 Karl, T., Striednig, M., Graus, M., Hammerle, A., and Wohlfahrt, G.: Urban flux measurements reveal a large pool of oxygenated  
940 volatile organic compound emissions, *Proc. Natl. Acad. Sci. U.S.A.*, 115, 1186-1191, <https://doi.org/10.1073/pnas.1714715115>,  
941 2018.
- 942 Kaser, L., Karl, T., Schnitzhofer, R., Graus, M., Herdinger-Blatt, I. S., DiGangi, J. P., Sive, B., Turnipseed, A., Hornbrook, R.  
943 S., Zheng, W., Flocke, F. M., Guenther, A., Keutsch, F. N., Apel, E., and Hansel, A.: Comparison of different real time VOC



- 944 measurement techniques in a ponderosa pine forest, *Atmos. Chem. Phys.*, 13, 2893-2906, [https://doi.org/10.5194/acp-13-2893-](https://doi.org/10.5194/acp-13-2893-2013)  
945 2013, 2013.
- 946 Kim, M. J., Novak, G. A., Zoerb, M. C., Yang, M. X., Blomquist, B. W., Huebert, B. J., Cappa, C. D., and Bertram, T. H.: Air-  
947 Sea exchange of biogenic volatile organic compounds and the impact on aerosol particle size distributions, *Geophys Res Lett*, 44,  
948 3887-3896, <https://doi.org/10.1002/2017GL072975>, 2017.
- 949 Kim, P. S., Jacob, D. J., Fisher, J. A., Travis, K., Yu, K., Zhu, L., Yantosca, R. M., Sulprizio, M. P., Jimenez, J. L., Campuzano-  
950 Jost, P., Froyd, K. D., Liao, J., Hair, J. W., Fenn, M. A., Butler, C. F., Wagner, N. L., Gordon, T. D., Welti, A., Wennberg, P. O.,  
951 Crounse, J. D., St Clair, J. M., Teng, A. P., Millet, D. B., Schwarz, J. P., Markovic, M. Z., and Perring, A. E.: Sources,  
952 seasonality, and trends of southeast US aerosol: an integrated analysis of surface, aircraft, and satellite observations with the  
953 GEOS-Chem chemical transport model, *Atmos. Chem. Phys.*, 15, 10411-10433, <https://doi.org/10.5194/acp-15-10411-2015>,  
954 2015.
- 955 Kim, S., Huey, L. G., Stickel, R. E., Tanner, D. J., Crawford, J. H., Olson, J. R., Chen, G., Brune, W. H., Ren, X., Leshner, R.,  
956 Wooldridge, P. J., Bertram, T. H., Perring, A., Cohen, R. C., Lefer, B. L., Shetter, R. E., Avery, M., Diskin, G., and Sokolik, I.:  
957 Measurement of HO<sub>2</sub>NO<sub>2</sub> in the free troposphere during the intercontinental chemical transport experiment - North America  
958 2004, *J. Geophys. Res. Atmos.*, 112, <https://doi.org/10.1029/2006jd007676>, 2007.
- 959 Kirkby, J., Duplissy, J., Sengupta, K., Frege, C., Gordon, H., Williamson, C., Heinritzi, M., Simon, M., Yan, C., Almeida, J.,  
960 Trostl, J., Nieminen, T., Ortega, I. K., Wagner, R., Adamov, A., Amorim, A., Bernhammer, A. K., Bianchi, F., Breitenlechner,  
961 M., Brilke, S., Chen, X., Craven, J., Dias, A., Ehrhart, S., Flagan, R. C., Franchin, A., Fuchs, C., Guida, R., Hakala, J., Hoyle, C.  
962 R., Jokinen, T., Junninen, H., Kangasluoma, J., Kim, J., Krapf, M., Kurten, A., Laaksonen, A., Lehtipalo, K., Makhmutov, V.,  
963 Mathot, S., Molteni, U., Onnela, A., Perakyla, O., Piel, F., Petaja, T., Praplan, A. P., Pringle, K., Rap, A., Richards, N. A.,  
964 Riipinen, I., Rissanen, M. P., Rondo, L., Sarnela, N., Schobesberger, S., Scott, C. E., Seinfeld, J. H., Sipila, M., Steiner, G.,  
965 Stozhkov, Y., Stratmann, F., Tome, A., Virtanen, A., Vogel, A. L., Wagner, A. C., Wagner, P. E., Weingartner, E., Wimmer, D.,  
966 Winkler, P. M., Ye, P., Zhang, X., Hansel, A., Dommen, J., Donahue, N. M., Worsnop, D. R., Baltensperger, U., Kulmala, M.,  
967 Carslaw, K. S., and Curtius, J.: Ion-induced nucleation of pure biogenic particles, *Nature*, 533, 521-526,  
968 <https://doi.org/10.1038/nature17953>, 2016.
- 969 Kroll, J. H., Donahue, N. M., Jimenez, J. L., Kessler, S. H., Canagaratna, M. R., Wilson, K. R., Altieri, K. E., Mazzoleni, L. R.,  
970 Wozniak, A. S., Bluhm, H., Mysak, E. R., Smith, J. D., Kolb, C. E., and Worsnop, D. R.: Carbon oxidation state as a metric for  
971 describing the chemistry of atmospheric organic aerosol, *Nat. Chem.*, 3, 133-139, <https://doi.org/10.1038/nchem.948>, 2011.
- 972 Lamarque, J. F., Bond, T. C., Eyring, V., Granier, C., Heil, A., Klimont, Z., Lee, D., Liousse, C., Mieville, A., Owen, B., Schultz,  
973 M. G., Shindell, D., Smith, S. J., Stehfest, E., Van Aardenne, J., Cooper, O. R., Kainuma, M., Mahowald, N., McConnell, J. R.,  
974 Naik, V., Riahi, K., and van Vuuren, D. P.: Historical (1850-2000) gridded anthropogenic and biomass burning emissions of  
975 reactive gases and aerosols: methodology and application, *Atmos. Chem. Phys.*, 10, 7017-7039, [https://doi.org/10.5194/acp-10-](https://doi.org/10.5194/acp-10-7017-2010)  
976 7017-2010, 2010.
- 977 Lee, B. H., Lopez-Hilfiker, F. D., Mohr, C., Kurten, T., Worsnop, D. R., and Thornton, J. A.: An iodide-adduct high-resolution  
978 time-of-flight chemical-ionization mass spectrometer: application to atmospheric inorganic and organic compounds, *Environ.*  
979 *Sci. Technol.*, 48, 6309-6317, <https://doi.org/10.1021/es500362a>, 2014.
- 980 Lerner, B. M., Gilman, J. B., Aikin, K. C., Atlas, E. L., Goldan, P. D., Graus, M., Hendershot, R., Isaacman-VanWertz, G. A.,  
981 Koss, A., Kuster, W. C., Lueb, R. A., McLaughlin, R. J., Peischl, J., Sueper, D., Ryerson, T. B., Tokarek, T. W., Warneke, C.,  
982 Yuan, B., and de Gouw, J. A.: An improved, automated whole air sampler and gas chromatography mass spectrometry analysis  
983 system for volatile organic compounds in the atmosphere, *Atmos. Meas. Tech.*, 10, 291-313, [https://doi.org/10.5194/amt-10-291-](https://doi.org/10.5194/amt-10-291-2017)  
984 2017, 2017.
- 985 Li, J., Mao, J., Min, K. E., Washenfelder, R. A., Brown, S. S., Kaiser, J., Keutsch, F. N., Volkamer, R., Wolfe, G. M., Hanisco, T.  
986 F., Pollack, I. B., Ryerson, T. B., Graus, M., Gilman, J. B., Lerner, B. M., Warneke, C., de Gouw, J. A., Middlebrook, A. M.,  
987 Liao, J., Welti, A., Henderson, B. H., McNeill, V. F., Hall, S. R., Ullmann, K., Donner, L. J., Paulot, F., and Horowitz, L. W.:  
988 Observational constraints on glyoxal production from isoprene oxidation and its contribution to organic aerosol over the  
989 Southeast United States, *J. Geophys. Res. Atmos.*, 121, 9849-9861, <https://doi.org/10.1002/2016JD025331>, 2016.
- 990 Li, S. M., Leithead, A., Moussa, S. G., Liggio, J., Moran, M. D., Wang, D., Hayden, K., Darlington, A., Gordon, M., Staebler, R.,  
991 Makar, P. A., Stroud, C. A., McLaren, R., Liu, P. S. K., O'Brien, J., Mittermeier, R. L., Zhang, J., Marson, G., Cober, S. G.,  
992 Wolde, M., and Wentzell, J. J. B.: Differences between measured and reported volatile organic compound emissions from oil  
993 sands facilities in Alberta, Canada, *Proc. Natl. Acad. Sci. U.S.A.*, 114, E3756-E3765, <https://doi.org/10.1073/pnas.1617862114>,  
994 2017.



- 995 Lin, J. T., and McElroy, M. B.: Impacts of boundary layer mixing on pollutant vertical profiles in the lower troposphere:  
996 Implications to satellite remote sensing, *Atmos. Environ.*, 44, 1726-1739, <https://doi.org/10.1016/j.atmosenv.2010.02.009>, 2010.
- 997 Lin, S. J., and Rood, R. B.: Multidimensional flux-form semi-Lagrangian transport schemes, *Mon Weather Rev*, 124, 2046-2070,  
998 [https://doi.org/10.1175/1520-0493\(1996\)124<2046:Mffslt>2.0.Co;2](https://doi.org/10.1175/1520-0493(1996)124<2046:Mffslt>2.0.Co;2), 1996.
- 999 Long, M., Yantosca, R., Nielsen, J., Keller, C., Da Silva, A., Sulprizio, M., Pawson, S., and Jacob, D.: Development of a grid-  
1000 independent GEOS-Chem chemical transport model (v9-02) as an atmospheric chemistry module for Earth system models,  
1001 *Geosci Model Dev*, 8, 595-602, 2015.
- 1002 Luo, G., and Yu, F.: A numerical evaluation of global oceanic emissions of alpha-pinene and isoprene, *Atmos. Chem. Phys.*, 10,  
1003 2007-2015, <https://doi.org/10.5194/acp-10-2007-2010>, 2010.
- 1004 Mao, J., Ren, X., Brune, W. H., Olson, J. R., Crawford, J. H., Fried, A., Huey, L. G., Cohen, R. C., Heikes, B., Singh, H. B.,  
1005 Blake, D. R., Sachse, G. W., Diskin, G. S., Hall, S. R., and Shetter, R. E.: Airborne measurement of OH reactivity during  
1006 INTEX-B, *Atmos. Chem. Phys.*, 9, 163-173, <https://doi.org/10.5194/acp-9-163-2009>, 2009.
- 1007 Marais, E. A., Jacob, D. J., Jimenez, J. L., Campuzano-Jost, P., Day, D. A., Hu, W., Krechmer, J., Zhu, L., Kim, P. S., Miller, C.  
1008 C., Fisher, J. A., Travis, K., Yu, K., Hanisco, T. F., Wolfe, G. M., Arkinson, H. L., Pye, H. O. T., Froyd, K. D., Liao, J., and  
1009 McNeill, V. F.: Aqueous-phase mechanism for secondary organic aerosol formation from isoprene: application to the southeast  
1010 United States and co-benefit of SO<sub>2</sub> emission controls, *Atmos. Chem. Phys.*, 16, 1603-1618, <https://doi.org/10.5194/acp-16-1603-2016>, 2016.
- 1012 Marandino, C. A., De Bruyn, W. J., Miller, S. D., Prather, M. J., and Saltzman, E. S.: Oceanic uptake and the global atmospheric  
1013 acetone budget, *Geophys Res Lett*, 32, <https://doi.org/10.1029/2005gl023285>, 2005.
- 1014 Mari, C., Jacob, D. J., and Bechtold, P.: Transport and scavenging of soluble gases in a deep convective cloud, *J. Geophys. Res.*  
1015 *Atmos.*, 105, 22255-22267, <https://doi.org/10.1029/2000jd900211>, 2000.
- 1016 McDonald, B. C., Gentner, D. R., Goldstein, A. H., and Harley, R. A.: Long-term trends in motor vehicle emissions in u.s. urban  
1017 areas, *Environ. Sci. Technol.*, 47, 10022-10031, <https://doi.org/10.1021/es401034z>, 2013.
- 1018 McDonald, B. C., de Gouw, J. A., Gilman, J. B., Jathar, S. H., Akherati, A., Cappa, C. D., Jimenez, J. L., Lee-Taylor, J., Hayes,  
1019 P. L., McKeen, S. A., Cui, Y. Y., Kim, S. W., Gentner, D. R., Isaacman-VanWertz, G., Goldstein, A. H., Harley, R. A., Frost, G.  
1020 J., Roberts, J. M., Ryerson, T. B., and Trainer, M.: Volatile chemical products emerging as largest petrochemical source of urban  
1021 organic emissions, *Science*, 359, 760-764, <https://doi.org/10.1126/science.aq0524>, 2018.
- 1022 Miller, C. C., Jacob, D. J., Marais, E. A., Yu, K. R., Travis, K. R., Kim, P. S., Fisher, J. A., Zhu, L., Wolfe, G. M., Hanisco, T. F.,  
1023 Keutsch, F. N., Kaiser, J., Min, K. E., Brown, S. S., Washenfelder, R. A., Abad, G. G., and Chance, K.: Glyoxal yield from  
1024 isoprene oxidation and relation to formaldehyde: chemical mechanism, constraints from SENEX aircraft observations, and  
1025 interpretation of OMI satellite data, *Atmos. Chem. Phys.*, 17, 8725-8738, <https://doi.org/10.5194/acp-17-8725-2017>, 2017.
- 1026 Millet, D. B., Jacob, D. J., Custer, T. G., de Gouw, J. A., Goldstein, A. H., Karl, T., Singh, H. B., Sive, B. C., Talbot, R. W.,  
1027 Warneke, C., and Williams, J.: New constraints on terrestrial and oceanic sources of atmospheric methanol, *Atmos. Chem. Phys.*,  
1028 8, 6887-6905, <https://doi.org/10.5194/acp-8-6887-2008>, 2008.
- 1029 Millet, D. B., Guenther, A., Siegel, D. A., Nelson, N. B., Singh, H. B., de Gouw, J. A., Warneke, C., Williams, J., Eerdekens, G.,  
1030 Sinha, V., Karl, T., Flocke, F., Apel, E., Riemer, D. D., Palmer, P. I., and Barkley, M.: Global atmospheric budget of  
1031 acetaldehyde: 3-D model analysis and constraints from in-situ and satellite observations, *Atmos. Chem. Phys.*, 10, 3405-3425,  
1032 <https://doi.org/10.5194/acp-10-3405-2010>, 2010.
- 1033 Millet, D. B., Apel, E., Henze, D. K., Hill, J., Marshall, J. D., Singh, H. B., and Tessum, C. W.: Natural and anthropogenic  
1034 ethanol sources in North America and potential atmospheric impacts of ethanol fuel use, *Environ. Sci. Technol.*, 46, 8484-8492,  
1035 <https://doi.org/10.1021/es300162u>, 2012.
- 1036 Millet, D. B., Baasandorj, M., Farmer, D. K., Thornton, J. A., Baumann, K., Brophy, P., Chaliyakunnel, S., de Gouw, J. A.,  
1037 Gaus, M., Hu, L., Koss, A., Lee, B. H., Lopez-Hilfiker, F. D., Neuman, J. A., Paulot, F., Peischl, J., Pollack, I. B., Ryerson, T.  
1038 B., Warneke, C., Williams, B. J., and Xu, J.: A large and ubiquitous source of atmospheric formic acid, *Atmos. Chem. Phys.*, 15,  
1039 6283-6304, <https://doi.org/10.5194/acp-15-6283-2015>, 2015.





- 1040 Millet, D. B., Alwe, H. D., Chen, X., Deventer, M. J., Griffis, T. J., Holzinger, R., Bertman, S. B., Rickly, P. S., Stevens, P. S.,  
1041 Leonardis, T., Locoge, N., Dusanter, S., Tyndall, G. S., Alvarez, S. L., Erickson, M. H., and Flynn, J. H.: Bidirectional  
1042 ecosystem-atmosphere fluxes of volatile organic compounds across the mass spectrum: How many matter?, *Acs Earth Space*  
1043 *Chem*, 2, 764-777, <https://doi.org/10.1021/acsearthspacechem.8b00061>, 2018.
- 1044 Min, K. E., Washenfelder, R. A., Dube, W. P., Langford, A. O., Edwards, P. M., Zarzana, K. J., Stutz, J., Lu, K., Rohrer, F.,  
1045 Zhang, Y., and Brown, S. S.: A broadband cavity enhanced absorption spectrometer for aircraft measurements of glyoxal,  
1046 methylglyoxal, nitrous acid, nitrogen dioxide, and water vapor, *Atmos. Meas. Tech.*, 9, 423-440, <https://doi.org/10.5194/amt-9-423-2016>, 2016.
- 1048 Müller, J. F., Liu, Z., Nguyen, V. S., Stavrou, T., Harvey, J. N., and Peeters, J.: The reaction of methyl peroxy and hydroxyl  
1049 radicals as a major source of atmospheric methanol, *Nat. Commun.*, 7, 13213, <https://doi.org/10.1038/ncomms13213>, 2016a.
- 1050 Müller, M., Mikoviny, T., Feil, S., Haidacher, S., Hanel, G., Hartungen, E., Jordan, A., Mark, L., Mutschlechner, P.,  
1051 Schottkowsky, R., Sulzer, P., Crawford, J. H., and Wisthaler, A.: A compact PTR-ToF-MS instrument for airborne measurements  
1052 of volatile organic compounds at high spatiotemporal resolution, *Atmos. Meas. Tech.*, 7, 3763-3772, <https://doi.org/10.5194/amt-7-3763-2014>, 2014.
- 1054 Müller, M., Anderson, B. E., Beyersdorf, A. J., Crawford, J. H., Diskin, G. S., Eichler, P., Fried, A., Keutsch, F. N., Mikoviny,  
1055 T., Thornhill, K. L., Walega, J. G., Weinheimer, A. J., Yang, M., Yokelson, R. J., and Wisthaler, A.: In situ measurements and  
1056 modeling of reactive trace gases in a small biomass burning plume, *Atmos. Chem. Phys.*, 16, 3813-3824,  
1057 <https://doi.org/10.5194/acp-16-3813-2016>, 2016b.
- 1058 Mungall, E. L., Abbatt, J. P. D., Wentzell, J. J. B., Lee, A. K. Y., Thomas, J. L., Blais, M., Gosselin, M., Miller, L. A.,  
1059 Papakyriakou, T., Willis, M. D., and Liggio, J.: Microlayer source of oxygenated volatile organic compounds in the summertime  
1060 marine Arctic boundary layer, *Proc. Natl. Acad. Sci. U.S.A.*, 114, 6203-6208, <https://doi.org/10.1073/pnas.1620571114>, 2017.
- 1061 Myhre, G., Shindell, D., Bréon, F.-M., Collins, W., Fuglestvedt, J., Huang, J., Koch, D., Lamarque, J.-F., Lee, D., Mendoza, B.,  
1062 Nakajima, T., Robock, A., Stephens, G., Takemura, T., and Zhang, H.: Anthropogenic and natural radiative forcing, in: *Climate*  
1063 *Change 2013: The Physical Science Basis. Contribution of Working Group I to the Fifth Assessment Report of the*  
1064 *Intergovernmental Panel on Climate Change*, edited by: Stocker, T. F., Qin, D., Plattner, G.-K., Tignor, M., Allen, S. K.,  
1065 Boschung, J., Nauels, A., Xia, Y., Bex, V., and Midgley, P. M., Cambridge University Press, Cambridge, United Kingdom and  
1066 New York, NY, USA, 659-740, 2013.
- 1067 Nguyen, T. B., Crounse, J. D., Teng, A. P., St Clair, J. M., Paulot, F., Wolfe, G. M., and Wennberg, P. O.: Rapid deposition of  
1068 oxidized biogenic compounds to a temperate forest, *Proc. Natl. Acad. Sci. U.S.A.*, 112, E392-401,  
1069 <https://doi.org/10.1073/pnas.1418702112>, 2015.
- 1070 Nirmalakhandan, N. N., and Speece, R. E.: QSAR model for predicting Henry's constant, *Environ. Sci. Technol.*, 22, 1349-1357,  
1071 <https://doi.org/10.1021/es00176a016>, 1988.
- 1072 O'Sullivan, D. W., Silwal, I. K. C., McNeill, A. S., Treadaway, V., and Heikes, B. G.: Quantification of gas phase hydrogen  
1073 peroxide and methyl peroxide in ambient air: Using atmospheric pressure chemical ionization mass spectrometry with O<sub>2</sub><sup>-</sup> and  
1074 O<sub>2</sub>-(CO<sub>2</sub>) reagent ions, *Int. J. Mass Spectrom.*, 424, 16-26, <https://doi.org/10.1016/j.ijms.2017.11.015>, 2018.
- 1075 Osthoff, H. D., Roberts, J. M., Ravishankara, A. R., Williams, E. J., Lerner, B. M., Sommariva, R., Bates, T. S., Coffman, D.,  
1076 Quinn, P. K., Dibb, J. E., Stark, H., Burkholder, J. B., Talukdar, R. K., Meagher, J., Fehsenfeld, F. C., and Brown, S. S.: High  
1077 levels of nitryl chloride in the polluted subtropical marine boundary layer, *Nat Geosci.*, 1, 324-328,  
1078 <https://doi.org/10.1038/ngeo177>, 2008.
- 1079 Palmer, P. I., and Shaw, S. L.: Quantifying global marine isoprene fluxes using MODIS chlorophyll observations, *Geophys Res*  
1080 *Lett.*, 32, <https://doi.org/10.1029/2005gl022592>, 2005.
- 1081 Park, J. H., Goldstein, A. H., Timkovsky, J., Fares, S., Weber, R., Karlik, J., and Holzinger, R.: Active atmosphere-ecosystem  
1082 exchange of the vast majority of detected volatile organic compounds, *Science*, 341, 643-647,  
1083 <https://doi.org/10.1126/science.1235053>, 2013.
- 1084 Parrish, D. D.: Critical evaluation of US on-road vehicle emission inventories, *Atmos. Environ.*, 40, 2288-2300,  
1085 <https://doi.org/10.1016/j.atmosenv.2005.11.033>, 2006.



- 1086 Paulot, F., Crounse, J. D., Kjaergaard, H. G., Kroll, J. H., Seinfeld, J. H., and Wennberg, P. O.: Isoprene photooxidation: new  
1087 insights into the production of acids and organic nitrates, *Atmos. Chem. Phys.*, 9, 1479-1501, [https://doi.org/10.5194/acp-9-1479-](https://doi.org/10.5194/acp-9-1479-2009)  
1088 2009, 2009a.
- 1089 Paulot, F., Crounse, J. D., Kjaergaard, H. G., Kurten, A., St Clair, J. M., Seinfeld, J. H., and Wennberg, P. O.: Unexpected  
1090 epoxide formation in the gas-phase photooxidation of isoprene, *Science*, 325, 730-733, [10.1126/science.1172910](https://doi.org/10.1126/science.1172910), 2009b.
- 1091 Paulot, F., Wunch, D., Crounse, J. D., Toon, G. C., Millet, D. B., DeCarlo, P. F., Vigouroux, C., Deutscher, N. M., Abad, G. G.,  
1092 Notholt, J., Warneke, T., Hannigan, J. W., Warneke, C., de Gouw, J. A., Dunlea, E. J., De Maziere, M., Griffith, D. W. T.,  
1093 Bernath, P., Jimenez, J. L., and Wennberg, P. O.: Importance of secondary sources in the atmospheric budgets of formic and  
1094 acetic acids, *Atmos. Chem. Phys.*, 11, 1989-2013, <https://doi.org/10.5194/acp-11-1989-2011>, 2011.
- 1095 Peischl, J., Ryerson, T. B., Holloway, J. S., Trainer, M., Andrews, A. E., Atlas, E. L., Blake, D. R., Daube, B. C., Dlugokencky,  
1096 E. J., Fischer, M. L., Goldstein, A. H., Guha, A., Karl, T., Kofler, J., Kosciuch, E., Misztal, P. K., Perring, A. E., Pollack, I. B.,  
1097 Santoni, G. W., Schwarz, J. P., Spackman, J. R., Wofsy, S. C., and Parrish, D. D.: Airborne observations of methane emissions  
1098 from rice cultivation in the Sacramento Valley of California, *J. Geophys. Res. Atmos.*, 117, n/a-n/a,  
1099 <https://doi.org/10.1029/2012jd017994>, 2012.
- 1100 Pfister, G., Flocke, F., Hornbrook, R., Orlando, J., Lee, S., and Schroeder, J.: FRAPPÉ Final Report: Process-Based and Regional  
1101 Source Impact Analysis for FRAPPÉ and DISCOVER-AQ 2014, available at:  
1102 [https://www.colorado.gov/airquality/tech\\_doc\\_repository.aspx?action=open&file=FRAPPE-NCAR\\_Final\\_Report\\_July2017.pdf](https://www.colorado.gov/airquality/tech_doc_repository.aspx?action=open&file=FRAPPE-NCAR_Final_Report_July2017.pdf),  
1103 last access: 13 Jan 2019, 2017.
- 1104 Philip, S., Martin, R. V., and Keller, C. A.: Sensitivity of chemistry-transport model simulations to the duration of chemical and  
1105 transport operators: a case study with GEOS-Chem v10-01, *Geosci Model Dev*, 9, 1683-1695, [https://doi.org/10.5194/gmd-9-](https://doi.org/10.5194/gmd-9-1683-2016)  
1106 1683-2016, 2016.
- 1107 Pollack, I. B., Lerner, B. M., and Ryerson, T. B.: Evaluation of ultraviolet light-emitting diodes for detection of atmospheric NO<sub>2</sub>  
1108 by photolysis - chemiluminescence, *J. Atmos. Chem.*, 65, 111-125, <https://doi.org/10.1007/s10874-011-9184-3>, 2010.
- 1109 Praske, E., Otkjaer, R. V., Crounse, J. D., Hethcox, J. C., Stoltz, B. M., Kjaergaard, H. G., and Wennberg, P. O.: Atmospheric  
1110 autoxidation is increasingly important in urban and suburban North America, *Proc. Natl. Acad. Sci. U.S.A.*, 115, 64-69,  
1111 <https://doi.org/10.1073/pnas.1715540115>, 2018.
- 1112 Read, K. A., Mahajan, A. S., Carpenter, L. J., Evans, M. J., Faria, B. V., Heard, D. E., Hopkins, J. R., Lee, J. D., Moller, S. J.,  
1113 Lewis, A. C., Mendes, L., McQuaid, J. B., Oetjen, H., Saiz-Lopez, A., Pilling, M. J., and Plane, J. M.: Extensive halogen-  
1114 mediated ozone destruction over the tropical Atlantic Ocean, *Nature*, 453, 1232-1235, <https://doi.org/10.1038/nature07035>, 2008.
- 1115 Read, K. A., Carpenter, L. J., Arnold, S. R., Beale, R., Nightingale, P. D., Hopkins, J. R., Lewis, A. C., Lee, J. D., Mendes, L.,  
1116 and Pickering, S. J.: Multiannual observations of acetone, methanol, and acetaldehyde in remote tropical atlantic air: implications  
1117 for atmospheric OVOC budgets and oxidative capacity, *Environ. Sci. Technol.*, 46, 11028-11039,  
1118 <https://doi.org/10.1021/es302082p>, 2012.
- 1119 Riahi, K., Grubler, A., and Nakicenovic, N.: Scenarios of long-term socio-economic and environmental development under  
1120 climate stabilization, *Technol. Forecasting Social Change*, 74, 887-935, <https://doi.org/10.1016/j.techfore.2006.05.026>, 2007.
- 1121 Richter, D., Weibring, P., Walega, J. G., Fried, A., Spuler, S. M., and Taubman, M. S.: Compact highly sensitive multi-species  
1122 airborne mid-IR spectrometer, *Appl. Phys. B: Lasers Opt.*, 119, 119-131, <https://doi.org/10.1007/s00340-015-6038-8>, 2015.
- 1123 Ryerson, T. B., Buhr, M. P., Frost, G. J., Goldan, P. D., Holloway, J. S., Hubler, G., Jobson, B. T., Kuster, W. C., McKeen, S. A.,  
1124 Parrish, D. D., Roberts, J. M., Sueper, D. T., Trainer, M., Williams, J., and Fehsenfeld, F. C.: Emissions lifetimes and ozone  
1125 formation in power plant plumes, *J. Geophys. Res. Atmos.*, 103, 22569-22583, <https://doi.org/10.1029/98jd01620>, 1998.
- 1126 Ryerson, T. B., Huey, L. G., Knapp, K., Neuman, J. A., Parrish, D. D., Sueper, D. T., and Fehsenfeld, F. C.: Design and initial  
1127 characterization of an inlet for gas-phase NO<sub>y</sub> measurements from aircraft, *J. Geophys. Res. Atmos.*, 104, 5483-5492,  
1128 <https://doi.org/10.1029/1998jd100087>, 1999.
- 1129 Ryerson, T. B., Andrews, A. E., Angevine, W. M., Bates, T. S., Brock, C. A., Cairns, B., Cohen, R. C., Cooper, O. R., de Gouw,  
1130 J. A., Fehsenfeld, F. C., Ferrare, R. A., Fischer, M. L., Flagan, R. C., Goldstein, A. H., Hair, J. W., Hardesty, R. M., Hostetler, C.  
1131 A., Jimenez, J. L., Langford, A. O., McCauley, E., McKeen, S. A., Molina, L. T., Nenes, A., Oltmans, S. J., Parrish, D. D.,



- 1132 Pederson, J. R., Pierce, R. B., Prather, K., Quinn, P. K., Seinfeld, J. H., Senff, C. J., Sorooshian, A., Stutz, J., Surratt, J. D.,  
1133 Trainer, M., Volkamer, R., Williams, E. J., and Wofsy, S. C.: The 2010 California Research at the Nexus of Air Quality and  
1134 Climate Change (CalNex) field study, *J. Geophys. Res. Atmos.*, 118, 5830-5866, <https://doi.org/10.1002/jgrd.50331>, 2013.
- 1135 Safieddine, S. A., Heald, C. L., and Henderson, B. H.: The global nonmethane reactive organic carbon budget: A modeling  
1136 perspective, *Geophys Res Lett*, 44, 3897-3906, <https://doi.org/10.1002/2017GL072602>, 2017.
- 1137 Sander, R.: Compilation of Henry's law constants (version 4.0) for water as solvent, *Atmos. Chem. Phys.*, 15, 4399-4981,  
1138 <https://doi.org/10.5194/acp-15-4399-2015>, 2015.
- 1139 Schauffler, S. M., Atlas, E. L., Donnelly, S. G., Andrews, A., Montzka, S. A., Elkins, J. W., Hurst, D. F., Romashkin, P. A.,  
1140 Dutton, G. S., and Stroud, V.: Chlorine budget and partitioning during the Stratospheric Aerosol and Gas Experiment (SAGE) III  
1141 Ozone Loss and Validation Experiment (SOLVE), *J. Geophys. Res. Atmos.*, 108, <https://doi.org/10.1029/2001jd002040>, 2003.
- 1142 SEAC<sup>4</sup>RS Science Team: SEAC<sup>4</sup>RS Field Campaign Data. NASA Langley Atmospheric Science Data Center DAAC,  
1143 <https://doi.org/10.5067/aircraft/seac4rs/aerosol-tracegas-cloud>, 2013.
- 1144 Shaw, M. F., Sztáray, B., Whalley, L. K., Heard, D. E., Millet, D. B., Jordan, M. J., Osborn, D. L., and Kable, S. H.: Photo-  
1145 tautomerization of acetaldehyde as a photochemical source of formic acid in the troposphere, *Nat. Commun.*, 9, 2584, 2018.
- 1146 Shaw, S. L., Gantt, B., and Meskhidze, N.: Production and emissions of marine isoprene and monoterpenes: A review, *Adv  
1147 Meteorol*, 2010, 1-24, <https://doi.org/10.1155/2010/408696>, 2010.
- 1148 Singh, H. B., Tabazadeh, A., Evans, M. J., Field, B. D., Jacob, D. J., Sachse, G., Crawford, J. H., Shetter, R., and Brune, W. H.:  
1149 Oxygenated volatile organic chemicals in the oceans: Inferences and implications based on atmospheric observations and air-sea  
1150 exchange models, *Geophys Res Lett*, 30, <https://doi.org/10.1029/2003gl017933>, 2003.
- 1151 Slusher, D. L., Huey, L. G., Tanner, D. J., Flocke, F. M., and Roberts, J. M.: A thermal dissociation-chemical ionization mass  
1152 spectrometry (TD-CIMS) technique for the simultaneous measurement of peroxyacyl nitrates and dinitrogen pentoxide, *J.  
1153 Geophys. Res. Atmos.*, 109, <https://doi.org/10.1029/2004jd004670>, 2004.
- 1154 St Clair, J. M., McCabe, D. C., Crouse, J. D., Steiner, U., and Wennberg, P. O.: Chemical ionization tandem mass spectrometer  
1155 for the in situ measurement of methyl hydrogen peroxide, *Rev. Sci. Instrum.*, 81, 094102, <https://doi.org/10.1063/1.3480552>,  
1156 2010.
- 1157 Staudinger, J., and Roberts, P. V.: A critical compilation of Henry's law constant temperature dependence relations for organic  
1158 compounds in dilute aqueous solutions, *Chemosphere*, 44, 561-576, [https://doi.org/10.1016/S0045-6535\(00\)00505-1](https://doi.org/10.1016/S0045-6535(00)00505-1), 2001.
- 1159 Stavrakou, T., Muller, J. F., Peeters, J., Razavi, A., Clarisse, L., Clerbaux, C., Coheur, P. F., Hurtmans, D., De Maziere, M.,  
1160 Vigouroux, C., Deutsch, N. M., Griffith, D. W. T., Jones, N., and Paton-Walsh, C.: Satellite evidence for a large source of  
1161 formic acid from boreal and tropical forests, *Nat Geosci*, 5, 26-30, <https://doi.org/10.1038/NGEO1354>, 2012.
- 1162 Stettler, M. E. J., Eastham, S., and Barrett, S. R. H.: Air quality and public health impacts of UK airports. Part I: Emissions,  
1163 *Atmos. Environ.*, 45, 5415-5424, <https://doi.org/10.1016/j.atmosenv.2011.07.012>, 2011.
- 1164 Toon, O. B., Maring, H., Dibb, J., Ferrare, R., Jacob, D. J., Jensen, E. J., Luo, Z. J., Mace, G. G., Pan, L. L., Pfister, L., Rosenlof,  
1165 K. H., Redemann, J., Reid, J. S., Singh, H. B., Thompson, A. M., Yokelson, R., Minnis, P., Chen, G., Jucks, K. W., and Pszenny,  
1166 A.: Planning, implementation, and scientific goals of the Studies of Emissions and Atmospheric Composition, Clouds and  
1167 Climate Coupling by Regional Surveys (SEAC4RS) field mission, *J. Geophys. Res. Atmos.*, 121, 4967-5009,  
1168 <https://doi.org/10.1002/2015JD024297>, 2016.
- 1169 Travis, K. R., Jacob, D. J., Fisher, J. A., Kim, P. S., Marais, E. A., Zhu, L., Yu, K., Miller, C. C., Yantosca, R. M., Sulprizio, M.  
1170 P., Thompson, A. M., Wennberg, P. O., Crouse, J. D., St Clair, J. M., Cohen, R. C., Laughner, J. L., Dibb, J. E., Hall, S. R.,  
1171 Ullmann, K., Wolfe, G. M., Pollack, I. B., Peischl, J., Neuman, J. A., and Zhou, X.: Why do Models Overestimate Surface Ozone  
1172 in the Southeastern United States?, *Atmos. Chem. Phys.*, 16, 13561-13577, <https://doi.org/10.5194/acp-16-13561-2016>, 2016.
- 1173 Treadaway, V., Heikes, B. G., McNeill, A. S., Silwal, I. K. C., and O'Sullivan, D. W.: Measurement of formic acid, acetic acid  
1174 and hydroxyacetaldehyde, hydrogen peroxide, and methyl peroxide in air by chemical ionization mass spectrometry: airborne  
1175 method development, *Atmos Meas Tech*, 11, 1901-1920, [10.5194/amt-11-1901-2018](https://doi.org/10.5194/amt-11-1901-2018), 2018.



- 1176 Trostl, J., Chuang, W. K., Gordon, H., Heinritzi, M., Yan, C., Molteni, U., Ahlm, L., Frege, C., Bianchi, F., Wagner, R., Simon,  
1177 M., Lehtipalo, K., Williamson, C., Craven, J. S., Duplissy, J., Adamov, A., Almeida, J., Bernhammer, A. K., Breitenlechner, M.,  
1178 Brilke, S., Dias, A., Ehrhart, S., Flagan, R. C., Franchin, A., Fuchs, C., Guida, R., Gysel, M., Hansel, A., Hoyle, C. R., Jokinen,  
1179 T., Junninen, H., Kangasluoma, J., Keskinen, H., Kim, J., Krapf, M., Kurten, A., Laaksonen, A., Lawler, M., Leiminger, M.,  
1180 Mathot, S., Mohler, O., Nieminen, T., Onnela, A., Petaja, T., Piel, F. M., Miettinen, P., Rissanen, M. P., Rondo, L., Sarnela, N.,  
1181 Schobesberger, S., Sengupta, K., Sipila, M., Smith, J. N., Steiner, G., Tome, A., Virtanen, A., Wagner, A. C., Weingartner, E.,  
1182 Wimmer, D., Winkler, P. M., Ye, P. L., Carslaw, K. S., Curtius, J., Dommen, J., Kirkby, J., Kulmala, M., Riipinen, I., Worsnop,  
1183 D. R., Donahue, N. M., and Baltensperger, U.: The role of low-volatility organic compounds in initial particle growth in the  
1184 atmosphere, *Nature*, 533, 527–+, <https://doi.org/10.1038/nature18271>, 2016.
- 1185 van der Werf, G. R., Randerson, J. T., Giglio, L., van Leeuwen, T. T., Chen, Y., Rogers, B. M., Mu, M. Q., van Marle, M. J. E.,  
1186 Morton, D. C., Collatz, G. J., Yokelson, R. J., and Kasibhatla, P. S.: Global fire emissions estimates during 1997–2016, *Earth*  
1187 *Syst. Sci. Data*, 9, 697–720, <https://doi.org/10.5194/essd-9-697-2017>, 2017.
- 1188 van Vuuren, D. P., Edmonds, J., Kainuma, M., Riahi, K., Thomson, A., Hibbard, K., Hurtt, G. C., Kram, T., Krey, V., Lamarque,  
1189 J. F., Masui, T., Meinshausen, M., Nakicenovic, N., Smith, S. J., and Rose, S. K.: The representative concentration pathways: an  
1190 overview, *Clim. Change*, 109, 5–31, <https://doi.org/10.1007/s10584-011-0148-z>, 2011.
- 1191 Wang, Y. H., Jacob, D. J., and Logan, J. A.: Global simulation of tropospheric O<sub>3</sub>-NO<sub>x</sub>-hydrocarbon chemistry 1. Model  
1192 formulation, *J. Geophys. Res. Atmos.*, 103, 10713–10725, <https://doi.org/10.1029/98jd00158>, 1998.
- 1193 Warneke, C., de Gouw, J. A., Nowak, J. B., and Peischl, J.: Volatile organic compound emissions from agriculture in Central  
1194 Valley, California, *Abstr. Pap. Am. Chem. Soc.*, 242, 1, 2011.
- 1195 Warneke, C., de Gouw, J. A., Holloway, J. S., Peischl, J., Ryerson, T. B., Atlas, E., Blake, D., Trainer, M., and Parrish, D. D.:  
1196 Multiyear trends in volatile organic compounds in Los Angeles, California: Five decades of decreasing emissions, *J. Geophys.*  
1197 *Res. Atmos.*, 117, n/a–n/a, <https://doi.org/10.1029/2012jd017899>, 2012.
- 1198 Warneke, C., Geiger, F., Edwards, P. M., Dube, W., Petron, G., Kofler, J., Zahn, A., Brown, S. S., Graus, M., Gilman, J. B.,  
1199 Lerner, B. M., Peischl, J., Ryerson, T. B., de Gouw, J. A., and Roberts, J. M.: Volatile organic compound emissions from the oil  
1200 and natural gas industry in the Uintah Basin, Utah: oil and gas well pad emissions compared to ambient air composition, *Atmos.*  
1201 *Chem. Phys.*, 14, 10977–10988, <https://doi.org/10.5194/acp-14-10977-2014>, 2014.
- 1202 Warneke, C., Trainer, M., de Gouw, J. A., Parrish, D. D., Fahey, D. W., Ravishankara, A. R., Middlebrook, A. M., Brock, C. A.,  
1203 Roberts, J. M., Brown, S. S., Neuman, J. A., Lerner, B. M., Lack, D., Law, D., Hubler, G., Pollack, I., Sjostedt, S., Ryerson, T.  
1204 B., Gilman, J. B., Liao, J., Holloway, J., Peischl, J., Nowak, J. B., Aikin, K., Min, K. E., Washenfelder, R. A., Graus, M. G.,  
1205 Richardson, M., Markovic, M. Z., Wagner, N. L., Welti, A., Veres, P. R., Edwards, P., Schwarz, J. P., Gordon, T., Dube, W. P.,  
1206 McKeen, S., Brioude, J., Ahmadov, R., Bougiatioti, A., Lin, J. J., Nenes, A., Wolfe, G. M., Hanisco, T. F., Lee, B. H., Lopez-  
1207 Hilfiker, F. D., Thornton, J. A., Keutsch, F. N., Kaiser, J., Mao, J., and Hatch, C.: Instrumentation and measurement strategy for  
1208 the NOAA SENEX aircraft campaign as part of the Southeast Atmosphere Study 2013, *Atmos. Meas. Tech.*, 9, 3063–3093,  
1209 <https://doi.org/10.5194/amt-9-3063-2016>, 2016.
- 1210 Weibring, P., Richter, D., Walega, J. G., Rippe, L., and Fried, A.: Difference frequency generation spectrometer for simultaneous  
1211 multispecies detection, *Opt. Express*, 18, 27670–27681, <https://doi.org/10.1364/OE.18.027670>, 2010.
- 1212 Weinheimer, A. J., Walega, J. G., Ridley, B. A., Gary, B. L., Blake, D. R., Blake, N. J., Rowland, F. S., Sachse, G. W.,  
1213 Anderson, B. E., and Collins, J. E.: Meridional distributions of NO<sub>x</sub>, NO<sub>y</sub> and other species in the lower stratosphere and upper  
1214 troposphere during AASE II, *Geophys Res Lett*, 21, 2583–2586, <https://doi.org/10.1029/94gl01897>, 1994.
- 1215 Wells, K. C., Millet, D. B., Hu, L., Cady-Pereira, K. E., Xiao, Y., Shephard, M. W., Clerbaux, C. L., Clarisse, L., Coheur, P. F.,  
1216 Apel, E. C., de Gouw, J., Warneke, C., Singh, H. B., Goldstein, A. H., and Sive, B. C.: Tropospheric methanol observations from  
1217 space: retrieval evaluation and constraints on the seasonality of biogenic emissions, *Atmos. Chem. Phys.*, 12, 5897–5912,  
1218 <https://doi.org/10.5194/acp-12-5897-2012>, 2012.
- 1219 Wesely, M. L.: Parameterization of surface resistances to gaseous dry deposition in regional-scale numerical models, *Atmos.*  
1220 *Environ.*, 23, 1293–1304, [https://doi.org/10.1016/0004-6981\(89\)90153-4](https://doi.org/10.1016/0004-6981(89)90153-4), 1989.
- 1221 Wiedinmyer, C., Akagi, S. K., Yokelson, R. J., Emmons, L. K., Al-Saadi, J. A., Orlando, J. J., and Soja, A. J.: The Fire  
1222 INventory from NCAR (FINN): a high resolution global model to estimate the emissions from open burning, *Geosci Model Dev.*  
1223 4, 625–641, <https://doi.org/10.5194/gmd-4-625-2011>, 2011.



- 1224 Williams, J., Holzinger, R., Gros, V., Xu, X., Atlas, E., and Wallace, D. W. R.: Measurements of organic species in air and  
1225 seawater from the tropical Atlantic, *Geophys Res Lett*, 31, <https://doi.org/10.1029/2004gl020012>, 2004.
- 1226 Wisthaler, A., Hansel, A., Dickerson, R. R., and Crutzen, P. J.: Organic trace gas measurements by PTR-MS during INDOEX  
1227 1999, *Journal of Geophysical Research*, 107, <https://doi.org/10.1029/2001jd000576>, 2002.
- 1228 Wolfe, G. M., Hanisco, T. F., Arkinson, H. L., Bui, T. P., Crounse, J. D., Dean-Day, J., Goldstein, A., Guenther, A., Hall, S. R.,  
1229 Huey, G., Jacob, D. J., Karl, T., Kim, P. S., Liu, X., Marvin, M. R., Mikoviny, T., Misztal, P. K., Nguyen, T. B., Peischl, J.,  
1230 Pollack, I., Ryerson, T., St Clair, J. M., Teng, A., Travis, K. R., Ullmann, K., Wennberg, P. O., and Wisthaler, A.: Quantifying  
1231 sources and sinks of reactive gases in the lower atmosphere using airborne flux observations, *Geophys Res Lett*, 42, 8231-8240,  
1232 <https://doi.org/10.1002/2015GL065839>, 2015.
- 1233 Wooldridge, P. J., Perring, A. E., Bertram, T. H., Flocke, F. M., Roberts, J. M., Singh, H. B., Huey, L. G., Thornton, J. A., Wolfe,  
1234 G. M., Murphy, J. G., Fry, J. L., Rollins, A. W., LaFranchi, B. W., and Cohen, R. C.: Total Peroxy Nitrates (EPNs) in the  
1235 atmosphere: the Thermal Dissociation-Laser Induced Fluorescence (TD-LIF) technique and comparisons to speciated PAN  
1236 measurements, *Atmos. Meas. Tech.*, 3, 593-607, <https://doi.org/10.5194/amt-3-593-2010>, 2010.
- 1237 Wu, S. L., Mickley, L. J., Jacob, D. J., Logan, J. A., Yantosca, R. M., and Rind, D.: Why are there large differences between  
1238 models in global budgets of tropospheric ozone?, *J. Geophys. Res. Atmos.*, 112, <https://doi.org/10.1029/2006jd007801>, 2007.
- 1239 Xiao, Y. P., Logan, J. A., Jacob, D. J., Hudman, R. C., Yantosca, R., and Blake, D. R.: Global budget of ethane and regional  
1240 constraints on US sources, *J. Geophys. Res. Atmos.*, 113, <https://doi.org/10.1029/2007jd009415>, 2008.
- 1241 Yacovitch, T. I., Herndon, S. C., Roscioli, J. R., Floerchinger, C., McGovern, R. M., Agnese, M., Petron, G., Kofler, J., Sweeney,  
1242 C., Karion, A., Conley, S. A., Kort, E. A., Nahle, L., Fischer, M., Hildebrandt, L., Koeth, J., McManus, J. B., Nelson, D. D.,  
1243 Zahniser, M. S., and Kolb, C. E.: Demonstration of an ethane spectrometer for methane source identification, *Environ. Sci.*  
1244 *Technol.*, 48, 8028-8034, <http://doi.org/10.1021/es501475q>, 2014.
- 1245 Yang, M., Nightingale, P. D., Beale, R., Liss, P. S., Blomquist, B., and Fairall, C.: Atmospheric deposition of methanol over the  
1246 Atlantic Ocean, *Proc. Natl. Acad. Sci. U.S.A.*, 110, 20034-20039, <https://doi.org/10.1073/pnas.1317840110>, 2013.
- 1247 Yang, M., Beale, R., Liss, P., Johnson, M., Blomquist, B., and Nightingale, P.: Air-sea fluxes of oxygenated volatile organic  
1248 compounds across the Atlantic Ocean, *Atmos. Chem. Phys.*, 14, 7499-7517, <https://doi.org/10.5194/acp-14-7499-2014>, 2014a.
- 1249 Yang, M. X., Blomquist, B. W., and Nightingale, P. D.: Air-sea exchange of methanol and acetone during HiWinGS: Estimation  
1250 of air phase, water phase gas transfer velocities, *J. Geophys. Res. Oceans*, 119, 7308-7323,  
1251 <https://doi.org/10.1002/2014JC010227>, 2014b.
- 1252 Yevich, R., and Logan, J. A.: An assessment of biofuel use and burning of agricultural waste in the developing world, *Global*  
1253 *Biogeochem Cy*, 17, <https://doi.org/10.1029/2002gb001952>, 2003.
- 1254 Yu, K., Keller, C. A., Jacob, D. J., Molod, A. M., Eastham, S. D., and Long, M. S.: Errors and improvements in the use of  
1255 archived meteorological data for chemical transport modeling: an analysis using GEOS-Chem v11-01 driven by GEOS-5  
1256 meteorology, *Geosci Model Dev*, 11, 305-319, [10.5194/gmd-11-305-2018](https://doi.org/10.5194/gmd-11-305-2018), 2018.
- 1257 Yu, K. R., Jacob, D. J., Fisher, J. A., Kim, P. S., Marais, E. A., Miller, C. C., Travis, K. R., Zhu, L., Yantosca, R. M., Sulprizio,  
1258 M. P., Cohen, R. C., Dibb, J. E., Fried, A., Mikoviny, T., Ryerson, T. B., Wennberg, P. O., and Wisthaler, A.: Sensitivity to grid  
1259 resolution in the ability of a chemical transport model to simulate observed oxidant chemistry under high-isoprene conditions,  
1260 *Atmos. Chem. Phys.*, 16, 4369-4378, [10.5194/acp-16-4369-2016](https://doi.org/10.5194/acp-16-4369-2016), 2016.
- 1261 Zheng, W., Flocke, F. M., Tyndall, G. S., Swanson, A., Orlando, J. J., Roberts, J. M., Huey, L. G., and Tanner, D. J.:  
1262 Characterization of a thermal decomposition chemical ionization mass spectrometer for the measurement of peroxy acyl nitrates  
1263 (PANs) in the atmosphere, *Atmos. Chem. Phys.*, 11, 6529-6547, <https://doi.org/10.5194/acp-11-6529-2011>, 2011.
- 1264 Zhou, X. L., and Mopper, K.: Photochemical production of low-molecular-weight carbonyl compounds in seawater and surface  
1265 microlayer and their air-sea exchange, *Mar. Chem.*, 56, 201-213, [https://doi.org/10.1016/S0304-4203\(96\)00076-X](https://doi.org/10.1016/S0304-4203(96)00076-X), 1997.
- 1266 Zhu, L., Jacob, D. J., Kim, P. S., Fisher, J. A., Yu, K., Travis, K. R., Mickley, L. J., Yantosca, R. M., Sulprizio, M. P., De Smedt,  
1267 I., Abad, G. G., Chance, K., Li, C., Ferrare, R., Fried, A., Hair, J. W., Hanisco, T. F., Richter, D., Scarino, A. J., Walega, J.,  
1268 Weibring, P., and Wolfe, G. M.: Observing atmospheric formaldehyde (HCHO) from space: validation and intercomparison of



1269 six retrievals from four satellites (OMI, GOME2A, GOME2B, OMPS) with SEAC(4)RS aircraft observations over the Southeast  
1270 US, Atmos. Chem. Phys., 16, 13477-13490, <https://doi.org/10.5194/acp-16-13477-2016>, 2016.

1271 Zhuang, J., Jacob, D. J., and Eastham, S. D.: The importance of vertical resolution in the free troposphere for modeling  
1272 intercontinental plumes, Atmos. Chem. Phys., 18, 6039-6055, 2018.

1273

1274 **Table 1. Overview of aircraft campaigns used here<sup>a</sup>.**

	Aircraft platform	Aircraft ceiling	Timeframe	Sampling region	Campaign overview and data DOI if applicable
CalNex	NOAA WP-3D	7600m	May – Jul 2010	California and offshore	Ryerson et al. (2013)
DC3	NASA DC-8	12500m	May – Jun 2012	Northeastern Colorado, west Texas to central Oklahoma, and northern Alabama	Barth et al. (2015)
	NSF/NCAR GV	15500m		DC3 Science Team (2013)	
SENX	NOAA WP-3D	7600m	Jun – Jul 2013	Southeastern US	Warneke et al. (2016)
SEAC <sup>4</sup> RS	NASA DC-8	12500m	Aug – Sep 2013	Southeastern US and Gulf of Mexico	Toon et al. (2016) SEAC <sup>4</sup> RS Science Team (2013)
DISCOVER-AQ	NASA P-3B	8500m	Jun – Jul 2011	Baltimore-Washington, D.C.	Crawford and Pickering (2014)
			Jan – Feb 2013	San Joaquin Valley, California	DISCOVER-AQ Science Team (2014)
			Sep 2013	Houston, Texas	
			Jul – Aug 2014	Denver, Colorado	
FRAPPÉ	NCAR C-130	7900m	Jul – Aug 2014	Northern Colorado	Pfister et al. (2017)

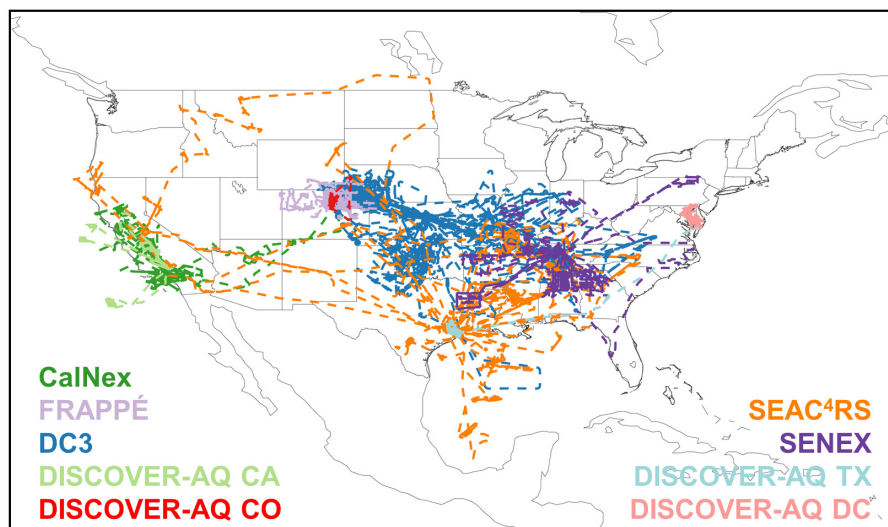
<sup>a</sup>See measurement details in Table S1 (O'Sullivan et al., 2018; Treadaway et al., 2018; Lerner et al., 2017; Min et al., 2016; Müller et al., 2016b; Cazorla et al., 2015; Richter et al., 2015; Lee et al., 2014; Müller et al., 2014; Yacovitch et al., 2014; Kaser et al., 2013; DiGangi et al., 2011; Fried et al., 2011; Zheng et al., 2011; Apel et al., 2010; Pollack et al., 2010; St Clair et al., 2010; Weibring et al., 2010; Wooldridge et al., 2010; Gilman et al., 2009; Hottle et al., 2009; Osthoff et al., 2008; de Gouw and Warneke, 2007; Huey, 2007; Kim et al., 2007; Crouse et al., 2006; Slusher et al., 2004; Blake et al., 2003; Schauffler et al., 2003; Wisthaler et al., 2002; Colman et al., 2001; Ryerson et al., 1999; Ryerson et al., 1998; Weinheimer et al., 1994).

1275

1276

1277

1278

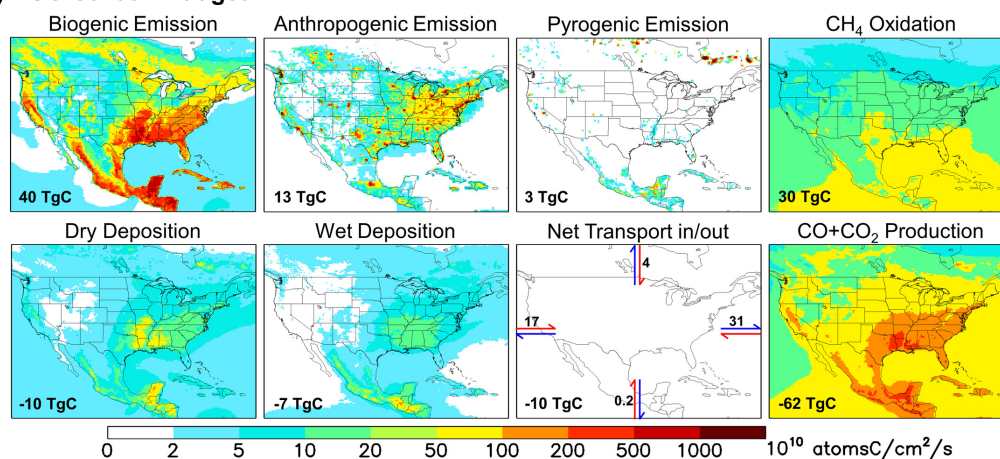


1279

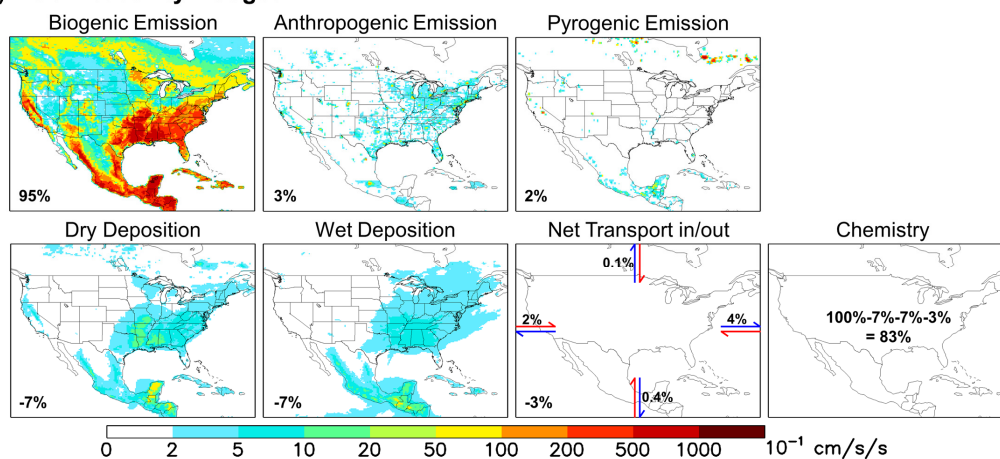
1280 **Figure 1. Flight tracks for the aircraft campaigns used in this study: CalNex (May-Jun 2010), FRAPPÉ (Jul-**  
 1281 **Aug 2014), DC3 (May-Jun 2012), DISCOVER-AQ CA (Jan-Feb 2013), DISCOVER-AQ CO (Jul-Aug 2014),**  
 1282 **SEAC<sup>4</sup>RS (Aug-Sep 2013), SENEX (Jun 2013), DISCOVER-AQ TX (Sep 2013), and DISCOVER-AQ DC**  
 1283 **(Jun-Jul 2011).**



**(a) VOC Carbon Budget**



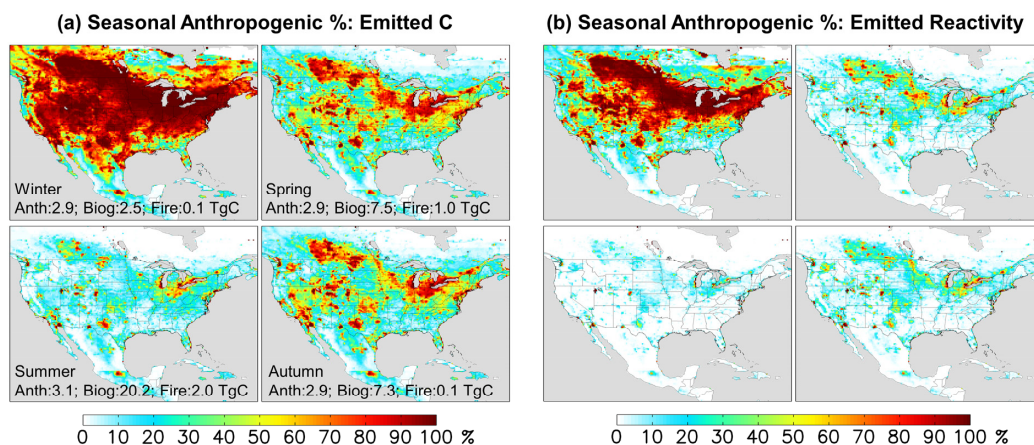
**(b) VOC Reactivity Budget**



1284

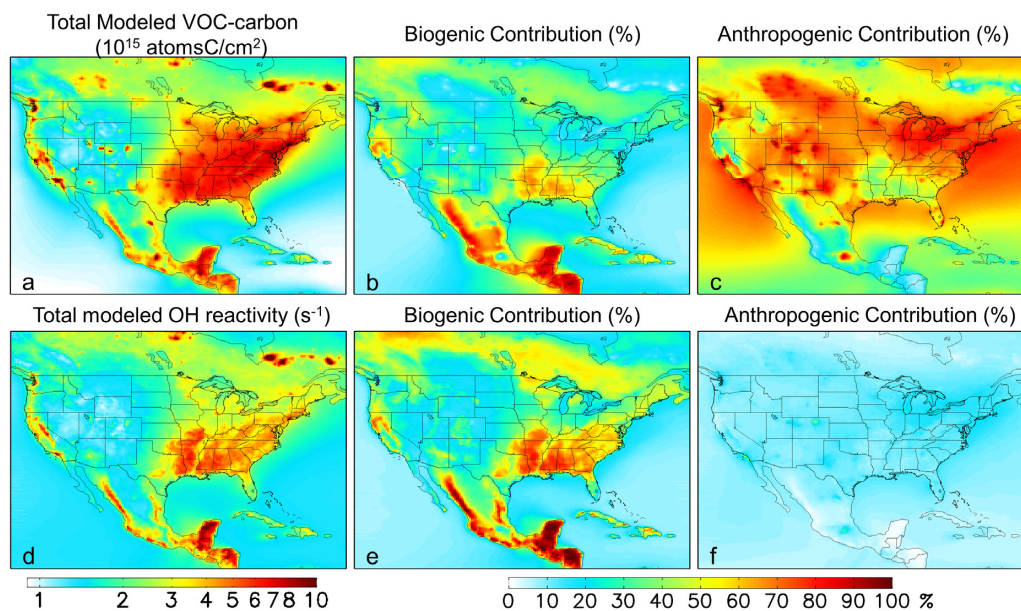
1285 **Figure 2.** Annual VOC-carbon (a) and reactivity (b) budgets over North America as simulated by GEOS-  
 1286 Chem for 2013. For panel (a) the annually integrated flux for each source/sink is given inset. For panel (b) all  
 1287 VOC fluxes are weighted by the corresponding OH reaction rate coefficient at 298 K to derive a VOC  
 1288 reactivity budget. Values inset indicating the fraction of total emitted reactivity produced or removed by that  
 1289 source/sink/transport process.





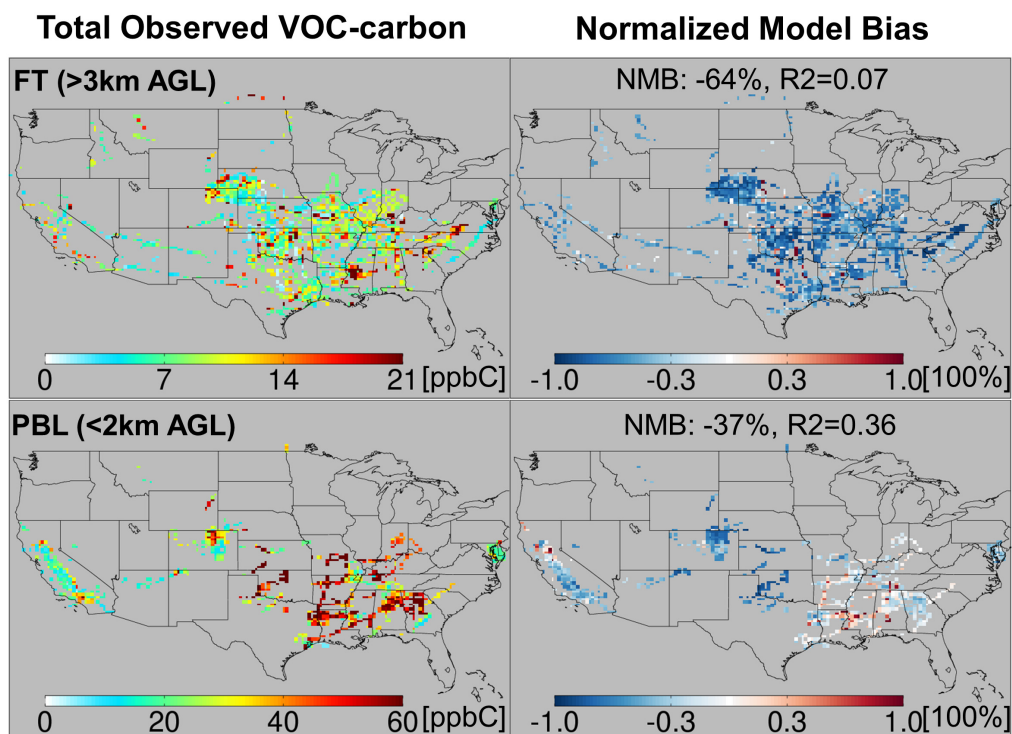
1290  
 1291  
 1292  
 1293  
 1294  
 1295

**Figure 3. Seasonal anthropogenic contribution to total VOC-carbon emissions (panel a) and to total reactivity-weighted VOC emissions (panel b). Numbers inset indicate the domain-wide contribution from anthropogenic, biogenic, and biomass burning sources.**



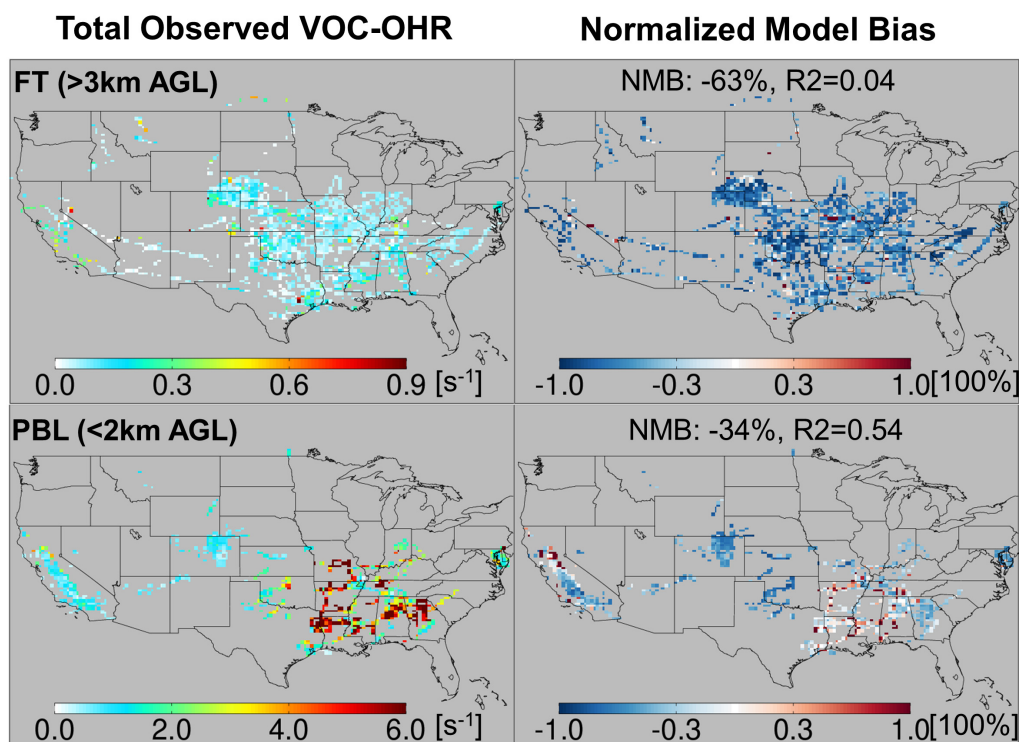
1296  
 1297  
 1298  
 1299  
 1300  
 1301  
 1302

**Figure 4. Distribution and source attribution of ambient VOC-carbon and associated OH reactivity over North America. Panels (a) and (d): total VOC-carbon and VOC-driven OH reactivity as simulated in the lowest model layer (below ~130m). Panel (b) and (e): ambient VOC-carbon and reactivity attributed to biogenic VOC emissions. Panel (c) and (f): ambient VOC-carbon and reactivity attributed to anthropogenic VOC emissions. Source attributions are derived based on model sensitivity tests with 10% modified anthropogenic or biogenic emissions, as described in-text.**



1303

1304 **Figure 5.** Total observed VOC-carbon loading (left) over North America in the planetary boundary layer (<2  
1305 km AGL) and free troposphere (>3 km AGL). In the right-hand panels the GEOS-Chem model simulation is  
1306 compared to co-located aircraft observation with the normalized mean bias given inset. Note that the  
1307 sampling season and instrument payload vary among campaigns.

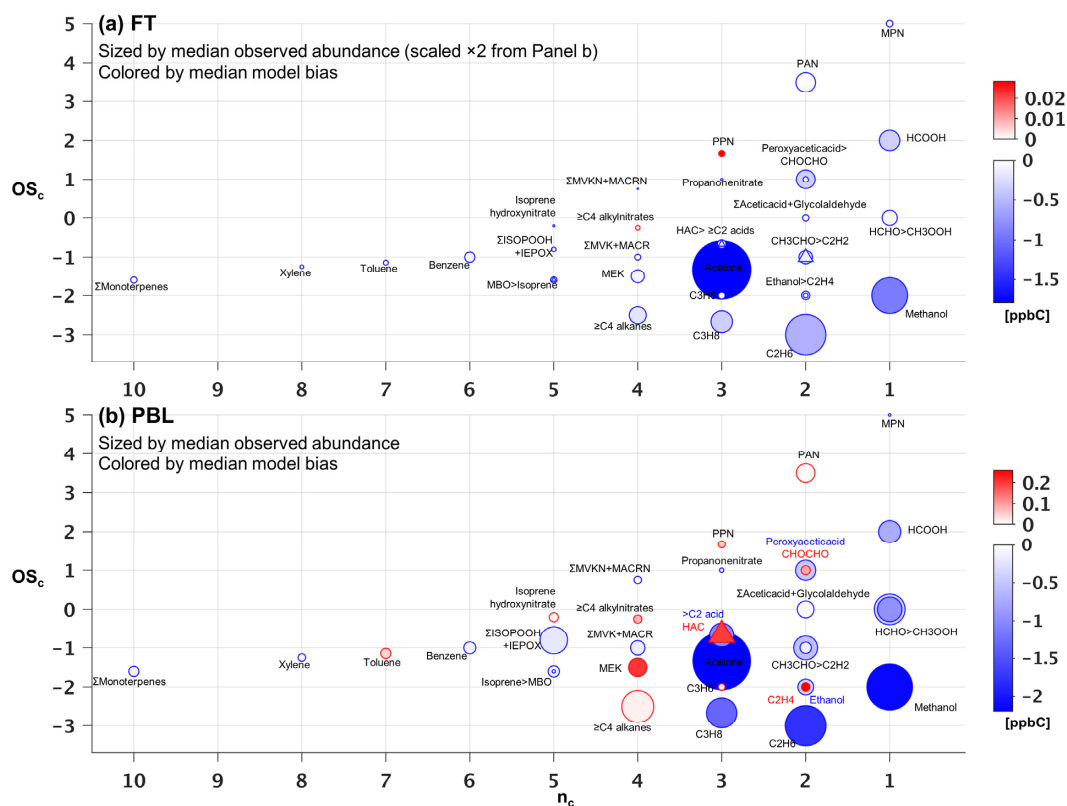


1308

1309 **Figure 6.** Total observed VOC reactivity (left) over North America in the planetary boundary layer (<2 km  
1310 AGL) and free troposphere (>3 km AGL). In the right-hand panels, the GEOS-Chem model simulation is  
1311 compared to co-located aircraft observation with the normalized mean bias given inset. Note that the  
1312 sampling season and instrument payload vary among campaigns.

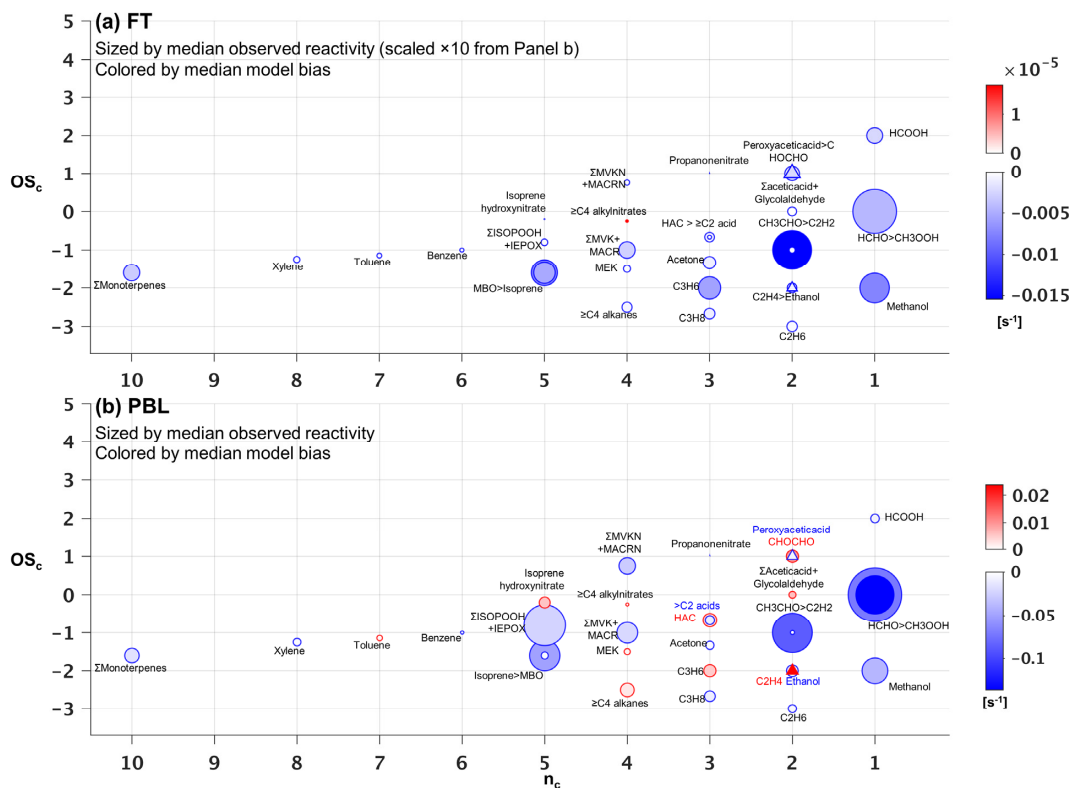


1313



1314

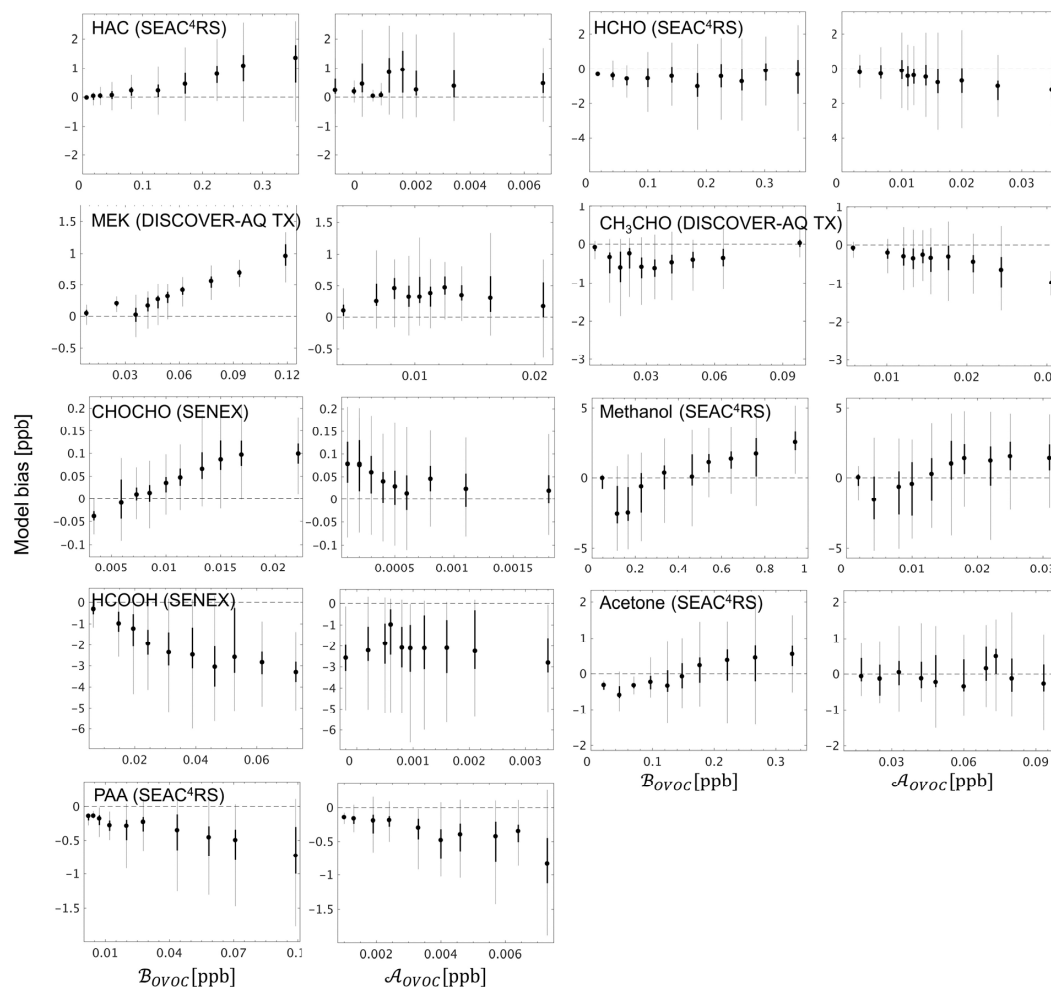
1315 **Figure 7. Observed versus predicted VOC-carbon as a function of carbon oxidation state ( $OS_c$ ) and number of carbon atoms ( $n_c$ ).**  
 1316 **Each circle indicates a single VOC (or lumped category for those that are measured or modeled collectively). Symbols are sized according to the observed median abundance (ppbC) of each species in the FT (panel a) and in the PBL (panel b, note altered size scaling from Panel a). Triangles are used when co-located circles are too close in size to distinguish, and symbols are colored according to the median**  
 1317 **absolute model bias in each case. For overlapping species, the more abundant of the two is indicated with “>”.**  
 1318  
 1319  
 1320



1321

1322 **Figure 8. Observed versus predicted VOC reactivity as a function of carbon oxidation state ( $OS_c$ ) and**  
 1323 **number of carbon atoms ( $n_c$ ). Each circle indicates a single VOC (or lumped category for those that are**  
 1324 **measured or modeled collectively). Symbols are sized according to the observed median reactivity ( $s^{-1}$ ) of each**  
 1325 **species in the FT (Panel a) and in the PBL (Panel b, note altered size scaling from Panel a). Triangles are used**  
 1326 **when co-located circles are too close to distinguish, and symbols are colored according to the median**  
 1327 **absolute model bias in each case. For overlapping species, the more abundant of the two is indicated with “>”.**





1334

1335  
 1336  
 1337  
 1338  
 1339  
 1340  
 1341

**Figure 10. GEOS-Chem model bias for select OVOCs in the boundary layer (<1 km here), binned according to the contribution from biogenic ( $B_{OVOC}$ ) and anthropogenic ( $A_{OVOC}$ ) sources to the overall abundance.  $B_{OVOC}$  and  $A_{OVOC}$  represent the integrated influence of primary + secondary biogenic and anthropogenic sources (respectively) for a given OVOC along the aircraft flight track based on the model simulation, as described in-text. The 10 plotted bins each represent an equal number of datapoints for a given OVOC, with the box plots indicating the corresponding median (filled circle), interquartile range (thick line), and 99% confidence interval (thin line).**